MAGNETIC AND ELECTROMAGNETIC CHARACTERIZATION OF BARIUM HEXAFERRITE CERAMICS AND THEIR POLYMER MATRIX COMPOSITES

A THESIS SUBMITTED TO
THE GRADUATE SCHOOL OF NATURAL AND APPLIED SCIENCES
OF
MIDDLE EAST TECHNICAL UNIVERSITY

BY

SERAY KAYA

IN PARTIAL FULFILLMENT OF THE REQUIREMENTS
FOR
THE DEGREE OF MASTER OF SCIENCE
IN
METALLURGICAL AND MATERIALS ENGINEERING

JUNE 2014

Approval of the thesis:

MAGNETIC AND ELECTROMAGNETIC CHARACTERIZATION OF BARIUM HEXAFERRITE CERAMICS AND THEIR POLYMER MATRIX COMPOSITES

submitted by **SERAY KAYA** in partial fulfillment of the requirements for the degree of **Master of Science in Metallurgical and Materials Engineering Department, Middle East Technical University** by,

Prof. Dr. Canan ÖZGEN _____
Dean, Graduate School of **Natural and Applied Sciences**

Prof. Dr. C. Hakan GÜR _____
Head of Department, **Metallurgical and Materials Engineering**

Assoc. Prof. Dr. Arcan Fehmi DERİCİOĞLU _____
Supervisor, **Metallurgical and Materials Engineering Dept. METU**

Prof. Dr. Abdullah ÖZTÜRK _____
Co-Supervisor, **Metallurgical and Materials Engineering Dept. METU**

Examining Committee Members:

Prof. Dr. Abdullah ÖZTÜRK _____
Metallurgical and Materials Eng. Dept. METU

Assoc. Prof. Dr. Arcan Fehmi DERİCİOĞLU _____
Metallurgical and Materials Eng. Dept. METU

Assoc. Prof. Dr. Caner DURUCAN _____
Metallurgical and Materials Eng. Dept. METU

Assoc. Prof. Dr. H.Emrah ÜNALAN _____
Metallurgical and Materials Eng. Dept. METU

Prof. Dr. Mehmet ERDOĞAN _____
Metallurgical and Materials Eng. Dept. GAZİ University

Date: 25.06.2014

I hereby declare that all information in this document has been obtained and presented in accordance with academic rules and ethical conduct. I also declare that, as required by these rules and conduct, I have fully cited and referenced all material and results that are not original to this work.

Name, Last name : Seray KAYA

Signature :

ABSTRACT

MAGNETIC AND ELECTROMAGNETIC CHARACTERIZATION
OF
BARIUM HEXAFERRITE CERAMICS AND THEIR POLYMER MATRIX
COMPOSITES

Kaya, Seray

M.Sc., Department of Metallurgical and Materials Engineering
Supervisor : Assoc. Prof. Dr. Arcan Fehmi DERİCİOĞLU
Co-Supervisor : Prof. Dr. Abdullah ÖZTÜRK

June 2014, 84 pages

In this study, BaHF-based polymer matrix composites were prepared as potential EM wave absorbing materials. Firstly, BaHF powders and platelets were synthesized by mixed oxide method and by molten salt synthesis (MSS) technique, respectively, which were further used as additives in the EM wave absorbing composites. The effect of molten salt composition on the amount of BaHF phase formation, as well as, on the morphology and magnetic properties of the final products were discussed according to the characterization results. Quantitative XRD results showed that with the increase in NaCl flux content, BaHF formation was enhanced and the highest conversion (97.8 wt%) was obtained in the case of 100 wt% NaCl flux. Corners of the BaHF platelets in NaCl flux were rounded, while KCl flux produced sharp edge platelets. Increasing NaCl content in the flux improved the coercivity and remnant magnetization of BaHF, leading to a more pronounced hard magnetic behavior.

In the second part of the study, BaHF-based polymer matrix composites were prepared by tape casting method, and their electromagnetic wave absorption potentials were investigated within 18-40 GHz frequency range by free-space measurement method. Effect of BaHF content and alignment on the EM wave properties was investigated. To enhance the EM wave absorption potential of the resulting composites, graphite or nickel flakes were incorporated into polymer matrix, and multilayered composites were produced. BaHF-Ni flake containing composites revealed ~50-75% EM wave absorption in 18-40 GHz range with the synergistic effect of the magnetic and ohmic loss effective in the structure.

Keywords: Barium Hexaferrite Ceramics, Mixed Oxide Method, Molten Salt Synthesis, Electromagnetic Wave Absorption, Polymer Matrix Composites.

ÖZ

BARYUM HEKZAFERRİT SERAMİKLERİNİN VE BARYUM HEKZAFERRİT POLİMER MATRİS KOMPOZİTLERİNİN MANYETİK VE ELEKTROMANYETİK KARAKTERİZASYONU

Kaya, Seray

Yüksek Lisans, Metalurji ve Malzeme Mühendisliği Bölümü
Tez Yöneticisi : Doç. Dr. Arcan Fehmi DERİCİOĞLU
Tez İkinci Danışmanı : Prof. Dr. Abdullah ÖZTÜRK

Haziran 2014, 84 sayfa

Bu çalışmada,EM dalga absorplama performansı için BaHF polimer matrisli kompozitler üretilmiştir. İlk olarak, BaHF tozu ve plakaları sırasıyla karışık oksit yöntemi ve eriyik tuz yöntemi ile üretilmiş ve sonrasında ise, elektromanyetik dalga sönümleyen kompozitlerde kullanılmıştır. Karakterizasyon sonuçlarından elde edilen veriler doğrultusunda, eriyik tuz kompozisyonunun oluşan BaHF'nin faz miktarına aynı zamanda da, morfoloji ve manyetik özelliklerine olan etkileri tartışılmıştır. Niceliksel X-Işınları Kırınımı sonuçları, NaCl tuz miktarının artışı ile BaHF faz oluşumunun arttığını ve en yüksek dönüşümün (ağırlıkça % 97.8) ağırlıkça % 100 NaCl tuzunda elde edildiğini göstermiştir. NaCl tuzunda, BaHF plakalarının köşeleri yuvarlak iken, KCl tuzu, keskin köşeli plakalar oluşturmuştur. Eriyik içerisindeki NaCl miktarının artışı, BaHF'nin koersivite ve remanent manyetizasyonunu iyileştirirp, daha kalıcı manyetik özelliklerin oluşumunu sağlamıştır.

Çalışmanın ikinci kısmında, şerit döküm yöntemi ile BaHF-polimer matrisli kompozitleri üretilmiştir ve serbest uzay yöntemi ile 18-40 GHz frekans aralığında elektromanyetik dalga sönümleme performansları ölçülmüştür. BaHF faz miktarının ve yönlenmesinin elektromanyetik dalga etkileşim özelliklerine etkileri incelenmiştir. Kompozitlerin elektromanyetik dalga sönümleme özelliklerini iyileştirmek amacıyla, polimer matrisi içerisine grafit ve nikel plakalar eklenmiş ve çok katmanlı kompozitler oluşturulmuştur. BaHF/Nikel içeren polimer matris kompozitleri, yapıdaki manyetik ve ohmik kayıpların etkisi ile 18-40 GHz frekans aralığında yaklaşık olarak 50-75 % EM dalga absorplama özelliği göstermiştir.

Anahtar Kelimeler: Baryum Hekzaferrit, Karışık Oksit Yöntemi, Eriyik Tuz Sentezi, Elektromanyetik Dalga Sönümleme, Polimer Matris Kompozitler

To My Family,

ACKNOWLEDGMENTS

I would like to express my sincere appreciation to Assoc. Prof. Dr. Arcan Dericioğlu for his supervision, guidance, support and encouragement throughout the study.

I am grateful to all the staff of the Department of Metallurgical and Materials Engineering and all my labmates Eda Aydoğan, Özgür Hamat, Aylin Güneş, Güney Daloğlu and Selen Güner for their moral support and friendship during my master's education.

Finally, I owe a depth to my family for their endless love, moral and monetary support and encouragement throughout my life.

TABLE OF CONTENTS

LIST OF TABLES

LIST OF FIGURES

CHAPTER 1

1. INTRODUCTION

Technological developments and innovations have necessitated widespread usage of the electromagnetic waves within a broad band frequency range. The electromagnetic waves are used in various civilian and military oriented application areas such as radars, telecommunications and wireless information transfer systems as well as medical diagnostic and research systems [1]. These applications operate at high frequencies and wide frequency bands where they should meet high performance, operational security and stability requirements. Interaction of emitted waves with the environment and with each other has become a growing social and industrial problem. These problems along with the operational requirements boosted the development of electromagnetic (EM) wave absorbing materials. In this context, research studies have been focused recently on the development of EM wave absorbing and interference shielding materials among which composites have attracted vast importance.

Composites made by dispersing metallic (nickel, silver, etc.) and nonmetallic (carbon) particles [1, 2] as well as stainless steel and carbon fibers [3-7] in epoxy type polymeric matrices are used as EM absorbing materials at different frequencies. Furthermore, particles like ferrites and nickel that provide magnetic loss could be used as EM wave absorbing additive materials [1, 8, 9].

Among ferrites, barium hexaferrite (BaHF) with a chemical composition of $BaFe_{12}O_{19}$ has been used as an additive in EM wave absorbing composites due to its large saturation magnetization, high Curie temperature, excellent chemical stability, high corrosion resistance and easiness in processing [10].

Various processing methods such as the mixed oxide method [11], sol–gel process [11], hydrothermal synthesis [12], chemical co-precipitation [13], crystallization from a glassy precursor [13], spray-pyrolysis [14] and the molten salt synthesis (MSS) [15] have been utilized for the production of BaHF powders. These methods result in powders with varying particle sizes, morphologies, and magnetic properties.

Among these processing methods, MSS allows the low temperature synthesis of BaHF platelets starting from mixed oxides [15]. In this method, reactions can be completed in a relatively short time interval because of the short diffusion distances and high mobility of raw materials in molten salts, in addition to the high reactivity of the salts [16]. The MSS method was also shown to allow the preparation of complex oxide ceramics with anisometric morphologies [17, 18].

The purpose of the present study was to produce BaHF- based polymer matrix electromagnetic wave absorbing composites and to investigate their EM wave absorption properties in the 18-40 GHz frequency range. In order to accomplish this purpose, BaHF powders with nano meter in size were synthesized by mixed oxide method using barium carbonate and iron(III) oxide as the starting materials. Micron size BaHF platelets were prepared by the MSS method in various weight proportions of NaCl–KCl salt mixtures as a liquid medium. X-Ray diffraction analysis (XRD), scanning electron microscopy (SEM) and vibrating sample magnetometer (VSM) were used to identify the characteristics of the synthesized BaHF powders and platelets. The effect of molten salt composition on the amount of BaHF phase formation as well as on the morphology and magnetic properties of the final products were discussed in relation to the results obtained from the characterization studies.

In the scope of EM wave absorbing BaHF-based polymer matrix composite production efforts, BaHF powders and platelets were dispersed in PS matrix by tape casting method. Their EM wave absorption potentials were investigated within 18-40 GHz frequency range by free-space measurement method.

Effect of BaHF content on the EM wave absorption properties were investigated by adding varying amounts of BaHF powders or platelets into PS matrix. In order to improve the EM wave absorption potential of the resulting composites, in addition to BaHF powders graphite or nickel (Ni) flakes were incorporated into polymer matrix. Consequently, EM wave absorbing potential of multilayered BaHF-Graphite flake and BaHF-Ni flake composites were examined. The effect of the number of cascaded layers, and amount of additives, on the EM absorption properties of BaHF-Graphite flake and BaHF-Ni flake composites were investigated in 18-40 GHz frequency range.

In the following chapter (Chapter 2), basic principles related to interaction of EM waves with materials, types of EM absorbing materials, general information about ferrites, properties and crystal structure of BaHF is presented along with a brief related literature review. Third chapter covers the materials, production methods and characterization techniques utilized throughout this study. In the Results and Discussion chapter (Chapter 4), XRD, SEM and VSM data of BaHF powders and platelets are presented and achieved results are discussed. Effect of molten salt composition on the amount of BaHF phase formation as well as on the morphology and magnetic properties of the final products are discussed. Following that EM wave reflection, transmission and absorption properties of BaHF–based polymer matrix composites are presented. In this context, the effect of additive type and amount along with the number of cascaded layers on the EM absorption capabilities of BaHF-based polymer matrix composites are presented. Finally, highlights of the current study are given in the Conclusions chapter.

CHAPTER 2

2. LITERATURE REVIEW

2.1. Interaction of Electromagnetic Waves with Materials

The electromagnetic waves which propagate self-paced or spread from artificial sources are being used in several military and civilian areas, for instance radars, telecommunications, wireless information transfer systems. They are even being used in medical diagnostic and research systems. As a result of the advances in technology, electromagnetic waves with centimeter and millimeter wavelengths are being used widespread and the interaction of emitted waves with the environment and with each other has become a growing problem.

Operating at high frequencies and wide frequency bands, the above mentioned applications need to satisfy both high performance and operational security along with specific stability requirements, which renders the development of electromagnetic wave absorbing materials crucial. In this context, in recent years researches have been focused on the development of electromagnetic (EM) wave absorbing and interference shielding materials.

The main function of EM wave absorbing materials is to limit the energy in distinct areas and definite values or to hinder the wide spreading of waves [19]. In Figure 2.1, the interaction between electromagnetic wave and a target material is schematically illustrated.

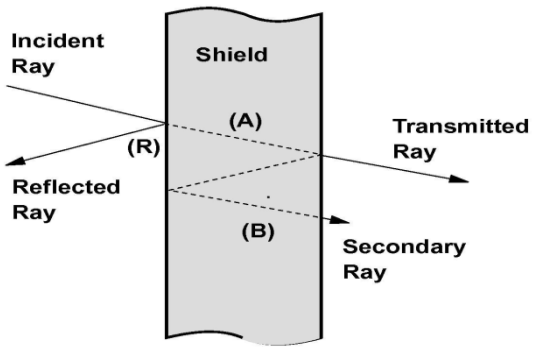

Figure 2.1 EM wave shielding mechanism in materials [20].

2.2. Electromagnetic Wave Absorbing Materials

A material to be used as an electromagnetic wave absorber, it should damp or dissipate the electromagnetic energy effectively. This condition occurs by the ohmic loss due to transport of charged particles (electrons and/or ions) or by dielectric (molecular) polarization loss and/or by magnetic polarization losses [19]. The materials which satisfy these properties are named as "electromagnetic wave absorbing materials". According to their application areas, EM wave absorbing materials can be classified as radar absorbing materials (RAM), electromagnetic interference shielding (EMI) materials and materials used in high frequency communication lines.

2.2.1 Radar Absorbing Materials (RAMs)

The working principle of recent technology radars is that, one transmitter sends radio waves in pulses and these waves reach the target and reflect, so they are detected by a receiver [21].

From the reflected waves, receiver can analyze target's direction, distance and speed. There are two ways to lower the echo of the wave received from the target [22]. Studies carried have shown that the shape changes in target, changes its aerodynamic structure and also reduces its echo effectiveness. For this reason, studies have focused on the second way, namely EM wave absorbing materials. In this context, EM wave absorbing composites attracted some more attention due to some disadvantages of the monolithic materials used in EM wave absorption such as their heavy weights, low environmental resistance and deficient mechanical properties [23].

RAMs are designed to make the target undetectable by lowering its radar cross section (RCS) [21]. Generally, composite insulator materials, conductive particle polymers, ceramics and ferrites are used as RAMs [22-26]. The composites made by dispersing powder or fibrous type dielectric, metallic, carbon or ferrite materials in polymeric matrices can be applied on surfaces in the form of paints or tiles. In addition to these, ferrite type materials can be used as RAMs in the form of sintered tiles [29-34].

In all of these materials, the power of radar absorbing is related with the material's thickness, geometry and surface topography. In the case of the composite RAMs, this condition depends on the additive material's amount and dimension as well as the interaction between the additive and the matrix phases. Composites containing conducting metallic and/or nonmetallic particles (nickel, silver, carbon etc.) dispersed in epoxy type polymeric matrices [23, 32], as well as stainless steel and carbon fiber reinforced composites [33-37] can be used as EM wave absorbing materials at different frequencies. In addition to these, particles which provide magnetic loss like ferrites and nickel can also be used as EM wave absorbing additive materials [23, 38, 39].

2.2.1.1 Salisbury Screen

The first version of RAMs is known as “Salisbury Screen.” The thin screen of EM wave absorbing materials (such as glass-fiber cloth impregnated with a lossy resin containing graphite or carbon black) is placed at a distance which is an odd multiple of λ/4 (λ being the working design wavelength) from a metal surface constituting a quarter-wave window (Figure 2.2) [19]. If the distance between the thin screen and the metal surface is not λ/4, some of the incident wave is scattered. When this distance difference exceeds λ/4, the extent of the unwanted scattering also increases. Because of this, Salisbury screen is a material that works in a narrow frequency range being not a very useful one.

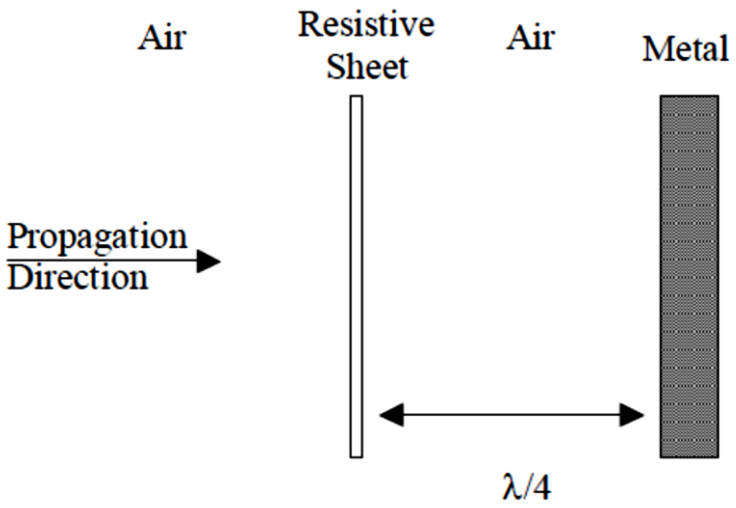

Figure 2.2 Schematic illustration of Salisbury screen [40].

2.2.1.2 Jaumann Absorber

Increasing the range of effective frequency band is possible with a material system that is composed of thin materials which are cascaded one after another in the form of distinct thin layers. The electrical resistance in the system decreases gradually through the material from the first layer to the last. This system is called a "Jaumann Absorber" (Figure 2.3). The frequency band coverage increases by the addition of thin layers with extra separators, which eventually increases the total thickness and hence the cost [21]. Because of such reasons, Jaumann Absorbers are usually not preferred in practice as EM wave absorbers.

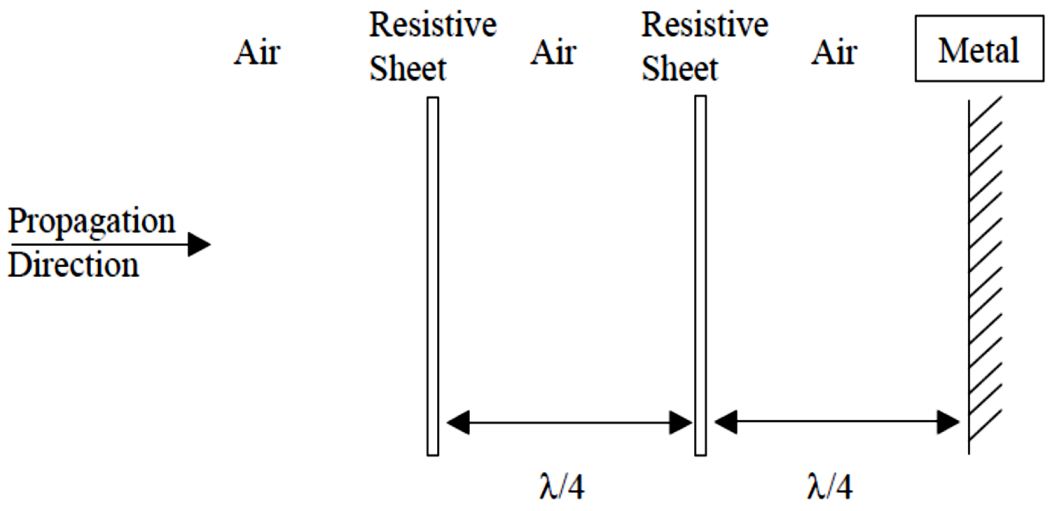

Figure 2.3. Schematic illustration of Jaumann Absorbers [40].

2.2.2 Magnetic Lossy Media

The absorber material can be replaced by a thinner one when a magnetic lossy material is incorporated into the structure. These materials are thinner when compared with dielectric containing ones. However, they are effective at lower frequency bands, and they have higher densities due to high content of iron.

The newly developed EM wave absorbing materials should work in wide frequency bands, and they should have low weight and good structural strength [41]. In this point of view, the ferrite containing polymer matrix composites are possible candidates for EM wave absorption applications.

Magnetic absorbers and lossy ferrite particles dispersed in a matrix are widely used in tailoring electromagnetic properties of polymers or polymer matrix composites [42]. Magnetic susceptibility and permanent magnetization provided by the ferromagnetic particles such as carbonyl iron, cobalt and nickel can also be utilized in such EM wave absorbing composites.

2.3 Ferrite Materials

Magnetic ceramics are made of ferrites, which are crystalline minerals composed of iron oxide in combination with some other metal. They are given the general formula $M(Fe_xO_y)$, M representing metallic elements other than iron [43]. Ferrites are classified into three groups according to their crystalline structure. These are Spinel, Garnet and Hexagonal Ferrites.

2.3.1 Spinel Ferrites

The ferrimagnetic oxides known as ferrites, have the general formula $M^{2+}O{\cdot}Fe_2{}^{3+}O_3$, where M^{2+} is a divalent metallic ion such as Fe^{2+}, N^{2+}, Cu^{2+}, Mg^{2+}. In the crystal structure, oxygen ions are in a nearly close-packed cubic array.

The unit cell contains 32 oxygen ions, with 32 octahedral sites and 64 tetrahedral sites; of these, 16 of the octahedral sites are filled (b sites), and 8 of the tetrahedral sites are filled (a sites), as illustrated in Figure 2.4.

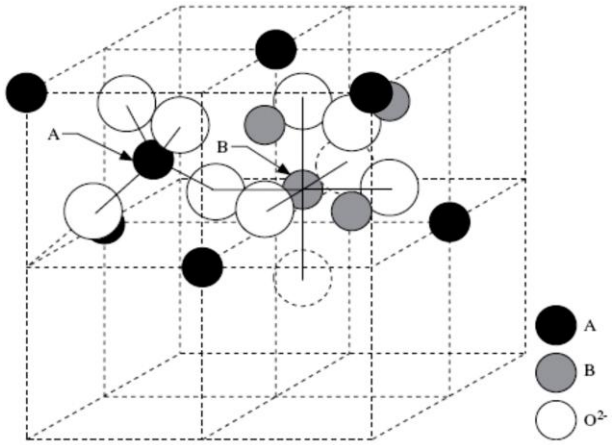

Figure 2.4 Two octants of the spinel unit cell, A and B represent tetrahedrally and octahedrally coordinated sites, respectively [44].

The antiparallel alignment and incomplete cancellation of magnetic spins between the two sublattices leads to a permanent magnetic moment. Because spinels are cubic in structure, with no preferred direction of magnetization, they are magnetically soft, i.e., it is relatively easy to change the direction of magnetization through the application of an external magnetic field [45]. Polycrystalline spinel ferrites have high electrical resistivity, chemical stability, mechanical hardness and reasonable cost, as a result of which they are widely used in various electronic devices [46].

2.3.2 Garnet Ferrites

They have the structure of the silicate mineral garnet and the chemical formula $M_3(Fe_5O_{12})$, where M is yttrium or a rare-earth trivalent cation. In addition to tetrahedral and octahedral sites, such as those seen in spinels, garnets have dodecahedral (12-coordinated) sites. The net ferrimagnetism is thus a complex result of antiparallel spin alignment among the three types of sites. Garnets are also magnetically hard [47].

2.3.3 Hexagonal Ferrites and BaHF

The hexagonal ferrites have a structure related to the spinel structure yet with hexagonal close-packed oxygen ions and a unit cell made up of two formulae of $AB_{12}O_{19}$, where A is divalent (Ba, Sr or Pb) and B is trivalent (Al, Ga, Cr or Fe), corresponding to a molecular formula $A^{2+}O{\cdot}B_2{}^{3+}O_3$. The best known example is magnetoplumbite, which has a formula $PbFe_{12}O_{19}$ and barium ferrite, $BaFe_{12}O_{19}$.

The barium ferrite structure consists of sections of the cubic spinel lattice (designated as S) separated by a hexagonal close-packed section (designated as R structure) containing the Ba-ion (Figure 2.5). Each S section consists of two layers of four oxygen ions, parallel to the hexagonal basal plane or (111) spinel planes, with three cations between each layer. The R section contains three layers of the hexagonal lattice, with one of the four oxygen ions in the center layer replaced by Ba. The unit cell consists of successive sections R, S, R*, S*, R, S and so on, in which * denotes a rotation of 180° about the hexagonal c axis or the <111> direction of the corresponding spinel lattice. The unit cell thus contains ten oxygen layers, with Ba replacing the oxygen ion every five layers. In a unit cell each S section has the formula Fe_6O_8 and each R section $BaFe_6O_{11}$. The total formula is $BaFe_{12}O_{19}$.

The Fe sites are tetrahedral and octahedral, and one site is surrounded by five oxygen ions forming a trigonal bipyramid [49]. This structure is illustrated in Figure 2.5.

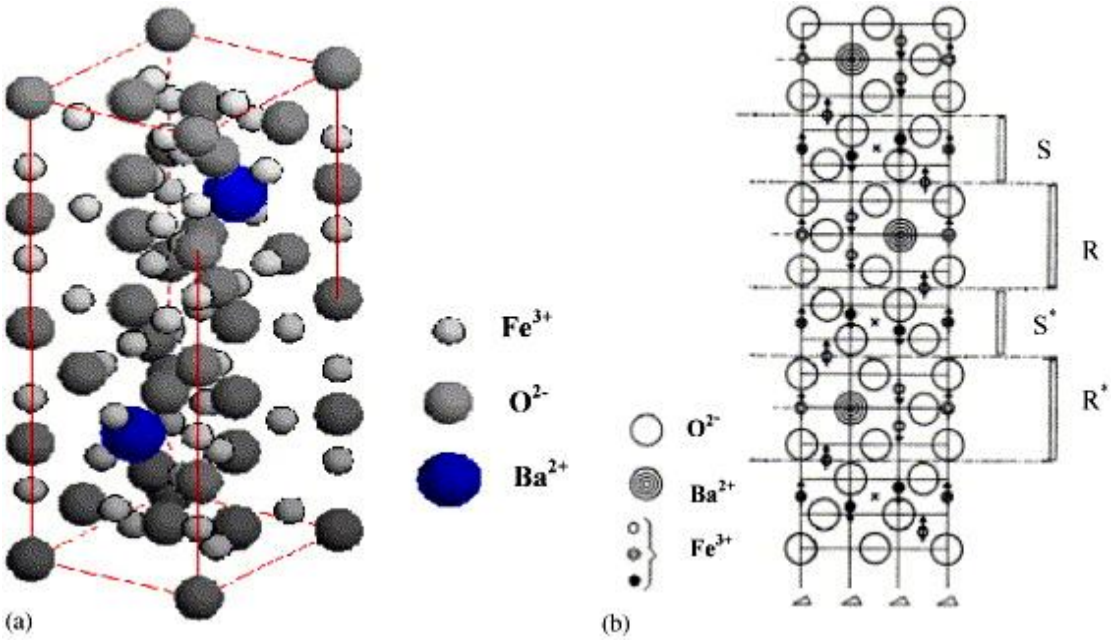

Figure 2.5 The structure of BaHF [50].

2.4 Types of Ferrites According to Their Magnetic Properties

As ceramics, ferrites are magnetic materials made by mixing iron oxide (Fe_2O_3) with other oxides and carbonates in the powdered form. The powders are then compacted and sintered at elevated temperatures. Sometimes finishing machining is necessary to produce the desired shape of the part [51].

Ferrites are classified into two groups according to their magnetic properties as soft and hard ferrites.

2.4.1 Magnetically Soft Ferrites

In soft ferrites there is a net magnetic moment due to two sets of unpaired inner-electron spin moments in opposite directions which do not cancel each other (Figure 2.6). This magnetism type is named as “ferrimagnetism”.

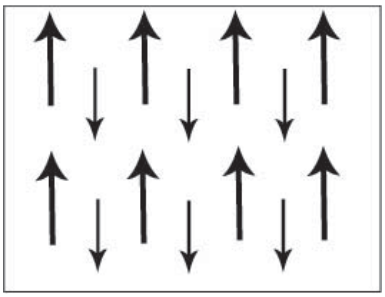

Figure 2.6. Electron spin moments of soft ferrites [52].

Soft ferrites are important magnetic materials, because in addition to having useful magnetic properties, they are insulators and have high electrical resistivities. Since they are insulators, they can be used in magnetic applications such as transformer cores which operate at high frequencies.

Some of the most important uses of soft ferrites are for low-signal, memory-core, audiovisual and recording-head applications. At low signal levels, soft ferrite cores are used for transformers and low-energy inductors [53].

2.4.2 Magnetically Hard Ferrites

A group of hard ferrites which are used for permanent magnets have the general formula $MO{\cdot}6Fe_2O_3$ and are hexagonal in crystal structure. The hexagonal ferrites are low in cost, low in density and have a high coercive force. The high magnetic strengths of these materials is due mainly to their high magnetocrystalline anisotropy [55]. The magnetization of these materials is believed to take place by domain wall nucleation and motion, as their grain size is too large for single-domain behavior.

Hard-ferrite permanent magnets find widespread use in generators, relays, and motors. Electronic applications include magnets for loudspeakers, telephone ringers, and receivers. They are also used for holding devices for door closers, seals and latches as well as in many toy designs [56].

The most important ferrite of this group is barium ferrite ($BaO{\cdot}6Fe_2O_3$), which was introduced in the Netherlands by the Philips Company in 1952 under the trade name Ferroxdure [54]. In recent years the barium ferrites have been replaced by the strontium ferrites to some extent, which have the general formula ($SrO{\cdot}6Fe_2O_3$) providing superior magnetic properties compared with the barium ferrites. These ferrites are produced by almost the same method used for the soft ferrites, with most being wet-pressed in a magnetic field to align the easy magnetizing axis of the particles with the applied field.

It has been found that the magnetization and anisotropic constant of strontium ferrite are greater than that of barium ferrite, and, furthermore, the Curie temperature is slightly higher. For this reason, strontium ferrite magnets have been the primary ferrite materials in commercial production since about 1980 [57].

It is known that the saturation magnetization and the anisotropy constant of PbO . $6Fe_20_3$ compound are lower than those of Sr and Ba ferrites, therefore, Pb ferrite magnets are not equivalent to ordinary Sr and Ba ferrite magnets as far as their magnetic properties are concerned [58]. More important than all of these issues, lead ferrites are toxic, as a result of which they do not have a wide use in ferrite industry.

2.5 Studies on Barium Ferrite Ceramics and Their Composites

M-type barium hexaferrites (BaHFs) ($BaFe_{12}O_{19}$) have attracted considerable attention because of their excellent magnetic properties and potential applications in various fields. As a hexaferrite, $BaFe_{12}O_{19}$ is one of the most frequently used ferrite in applications as permanent magnets [57].

In these type of ferrites the magnetic coercivity typically decreases with increasing crystallite size due to multi-domain formation and the easy movement of the domain walls [58].

Coercivity is also affected by the change of magnetocrystalline anisotropy. For strontium ferrite with hexagonal platelet-like morphology, when the c-axis is considered to be the easy-axis of magnetization, change of lattice parameter c would result in a decrease in coercivity. With the decrease of c (or c/a ratio), there is a decline in the degree of magnetocrystalline anisotropy and hence the reduction of coercivity [59].

Hexagonal ferrites having more permeability and higher magnetic resonance frequency than spinel ferrites are used as chip inductors and microwave absorbers in the GHz range [58]. Furthermore, due to their high saturation magnetization, great magnetic coercivity, high magnetocrystalline anisotropy field and excellent chemical stability, BaHFs are used in magnetic permanent and perpendicular recording media or electromagnetic wave absorption materials [59].

In this context, there are various studies reporting on the usage of BaHF powders as lossy additive in EM wave absorbing materials. In one of these studies Abbas et.al. [60] prepared Co^{2+}-Si^{4+} substituted BaHF polymer composites made of polyaniline and investigated their electromagnetic absorption properties at the 8.2-12.4 GHz range. The composites showed a minimum reflection loss of -29 dB at 10.97 GHz.

BaHF powders can be doped with various elements in order to improve their magnetic properties. In such a study pure and V_2O_5 doped $BaCo_xZn_2$-$xFe_{16}O_{27}$ barium ferrites where x=1.0, 1.3 and 1.5 were prepared by double-sintering method. The electromagnetic absorption results showed that when compared to undoped samples, 1.0 wt% V_2O_5 doped samples have about 50 % higher permeabilities which was explained by improved domain wall permeability [61].

BaHFs can be synthesized by various methods. Wu et.al. [41] prepared $BaMe_2Fe_{16}O_{27}$ by sol-gel method. Me_2 was selected as Co_2, CoNi and CoZn and obtained barium ferrites were blended with paraffin to make composites. The $BaCoZnFe_{16}O_{27}$/paraffin composite showed the best microwave absorption among the other two composites. Maximal reflection loss achieved was -16.23 dB.

In a study reported by Tehrani et. al. [62] $BaMg_{0.25}Mn_{0.25}Co_{0.5}Ti_{1.0}Fe_{10}O_{19}$ was prepared by solid state reaction method. Synthesized ferrite powders were incorporated in PVC matrix to form EM wave absorbing composites.

Vector network analyzer was used to investigate the EM wave absorption properties of the composites. At the 12-18 GHz frequency range, -40 dB maximum reflection loss was obtained.

In another study, undoped M-type BaHF prepared by reverse microemulsion technique was electromagnetically characterized in the 8-18 GHz ranges [63]. The minimum value of reflection loss reached was -28.52 dB at 13.80 GHz frequency.

2.6 Hysteresis Behavior of Magnetic Materials

The state of magnetization of a solid is a function of the strength and direction of the magnetizing field. If a magnetic material, which contains many small magnetic domains, not yet under an applied magnetic field is considered; the change in the domains as the field strength increasing can be examined using a typical magnetic field vs. magnetization (B-H) curve seen in Figure 2.7.

As the field is increased from zero, the effect on the solid is to displace domain boundaries in a reversible fashion. If the magnetic field is switched off, the domain boundaries return to their starting positions. Thus, the initial part of the B-H curve results from reversible domain boundary displacement, and the slope is called the "initial permeability, μ_i". As the magnetic field strength is increased, there is an irreversible boundary displacement, and at first the induced magnetization increases more rapidly than the field strength and gives a maximum slope, μ_{max}. Finally in the upper part of the magnetization curve all domain boundaries have been displaced, and further increase in the magnetic field causes rotation of the domains in the direction of the applied field. At this point the material is saturated where higher fields cannot induce more magnetization.

As the magnetic field is decreased to zero, the induced magnetization does not decrease to zero, as the alignment of most of the domains during magnetization results in a remnant magnetization or remanance, B_r.

When the direction of the magnetic field is reversed, the induced magnetization decreases and finally becomes zero at a value of the magnetic field strength called the coercive force, H_c. Further increased magnetic field strength in this opposite direction eventually causes magnetic saturation in the reverse direction and causes a saturation, B_s, and remanance, B_r, values of the same magnitude as in the first quadrant. As an applied field is cycled from one direction to the other direction, the hysteresis loop is followed.

Since the area of the hysteresis loop represents the energy or work to bring about changes in the magnetic domain structure, the product B·H, called the energy product, represents a net loss in the system, usually in the form of heat [66]. In applications in which the magnetic material is cycled around the magnetization curve many times per second, hysteresis losses are critical, and *soft* magnetic materials (with low B_r) are required.

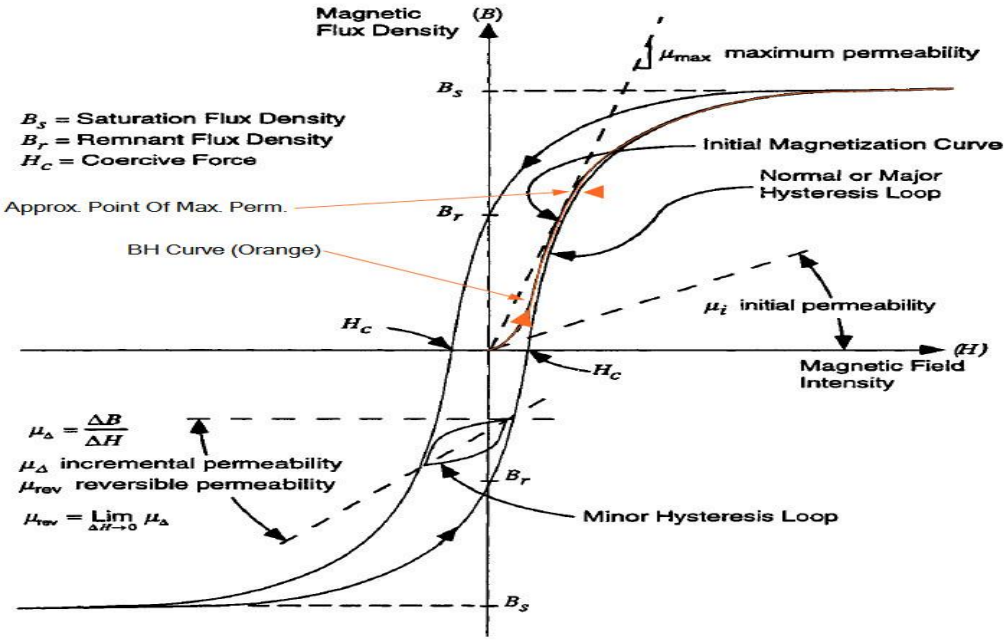

Figure 2.7. Typical hysteresis curve of a ferromagnetic material [67].

CHAPTER 3

3 EXPERIMENTAL PROCEDURE

3.1. General Procedure

BaHF powders and platelets were synthesized to fabricate BaHF-polymer matrix composites. Mixed oxide technique was used for the production of BaHF powders. BaHF platelets were produced by molten salt synthesis method. In both of the methods, the molar ratio of the initial materials Fe_2O_3 to $BaCO_3$ was 5.3 in order to complete the transformation to BaHF. This molar ratio was adopted from similar studies reported in literature [68, 69]. Mixed oxide method included two calcination steps. The first one was at 1040 ºC for 5 h and the following one was at 1050 ºC for 7 h. In the case of the molten salt synthesis, BaHF platelets were produced using five different compositions of NaCl and KCl molten salts at 900 ºC for 2 h.

BaHF-polymer matrix composites were fabricated by dispersing BaHF powders and platelets in the PS solution and then by tape casting this dispersion.

The average particle and platelet sizes were measured by applying quantitative metallographic analysis on the scanning electron microscope (FE-SEM, FEI 430 NanoSEM, Oregon, USA) images of the solid residues. Resulting solid residues were characterized by quantitative X-Ray analysis in order to determine the amount of BaHF formation.

Magnetic behavior of the synthesized BaHF powders and platelets were clarified via magnetic hysteresis curves obtained using vibrating sample magnetometer (VSM) (Cryogenic Limited PPMS, London, UK) at 300 K.

For the electromagnetic characterization of the BaHF-polymer matrix composites in the 18-40 GHz range free-space method was used in combination with a network analyzer.

3.2. Sample Preparation

3.2.1. Preparation of BaHF Powders by Mixed Oxide Method

Mixed oxide method was applied for the synthesis of BaHF powders. Reagent grade powders of Fe_2O_3 (Sigma-Aldrich, 99.999%) and $BaCO_3$ (Sigma-Aldrich, 99%) were used as the starting materials. Fe_2O_3 and $BaCO_3$ were mixed in Fe_2O_3/$BaCO_3$ molar ratio of 5.3. The starting materials were weighed in the required molar proportions and ball milled for 1.5 h in distilled water. Zirconia balls were used as the milling medium, where the ball to solid mixture weight ratio was 7. Water was added just to embed the ball and solid mixture in the polypropylene container. In order to remove the water from the mixture after ball milling, drying was applied in an oven at 80 ºC for 24 h. After this, the first calcination step was applied at 1040 ºC for 5 h in a muffle furnace in ambient air. Following the first calcination step, ball milling was applied using zirconia balls for 12 h in distilled water for further reduction of particle size. After applying the second drying at 80 ºC for 24 h, the second calcination step was done at 1050 ºC for 7 h to allow the completion of the below given reaction.

$$BaCO_3 + 6Fe_2O_3 = BaFe_{12}O_{19} + CO_2\ (g)$$

Synthesized BaHF powders were sieved utilizing 150 mesh sieve followed by ball milling at 375 rpm using zirconia balls for 12 h for the final particle size reduction.

Finally, BaHF powders with particle size ranging between 400 and 600 nm were achieved. These values were measured by applying quantitative metallographic analysis on the scanning electron microscope images.

Image J programme was used. Average of 20 different random particles were calculated and the standard deviation was 65 nm.

3.2.2. Preparation of BaHF Platelets by Molten Salt Synthesis Method

BaHF platelets were prepared by molten salt synthesis method. In this process, reagent grade powders of Fe_2O_3 (Sigma-Aldrich, 99.999%), $BaCO_3$ (Sigma-Aldrich, 99%), KCl (Sigma-Aldrich, 99%) and NaCl (Sigma-Aldrich, 99.5%) were used as starting materials. Fe_2O_3 and $BaCO_3$ were mixed to get $Fe_2O_3/BaCO_3$ molar ratio of 5.3. This ratio was selected from the Fe_2O_3-BaO binary phase diagram given in Figure 3.1.

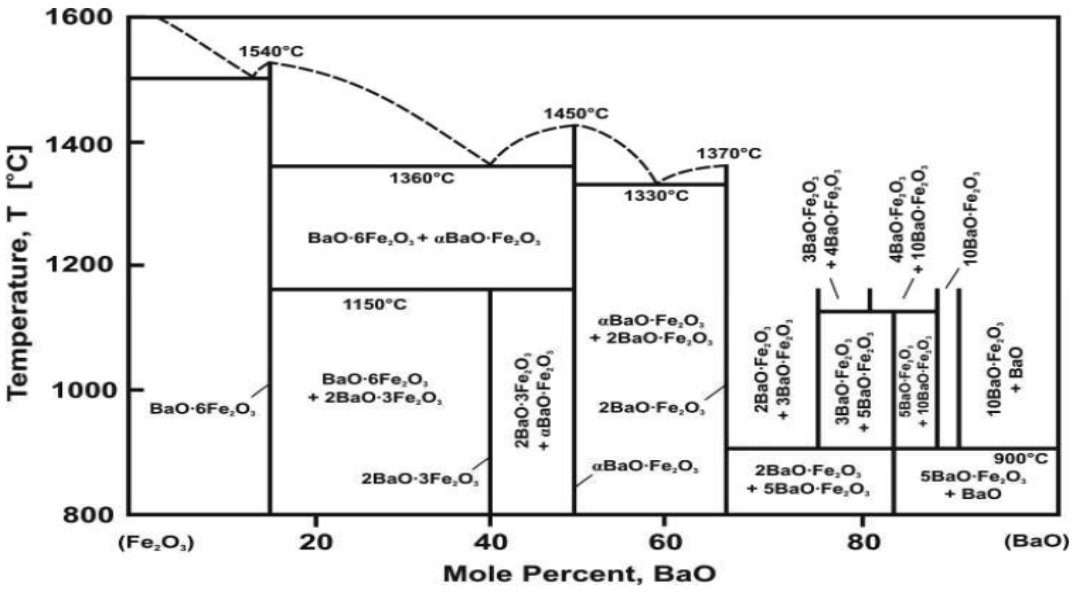

Figure 3.1. Binary phase diagram of Fe_2O_3-BaO including the obtained phases [69].

In order to investigate the effects of flux type and composition on the formation and morphology of BaHF platelets, $Fe_2O_3/BaCO_3$ mixtures with fixed molar ratio were added to the salt mixtures with the following compositions: 100 wt% NaCl, 90 wt% NaCl-10 wt% KCl, 44 wt% NaCl-56 wt% KCl, 90 wt% KCl and 100 wt% KCl. The initial mixtures comprised of 50 wt% flux and 50 wt% oxide/carbonate mixture (Fe_2O_3:$BaCO_3$= 5.3:1 mole) were calcined at 850, 900 and 950 ºC for 1, 2, 2.5 and 3.5 h. The calcination temperatures and flux compositions that were studied are shown on the NaCl-KCl binary phase diagram in Figure 3.2. After each calcination process, washing with distilled water and drying at 80 ºC in etuve for 24 h were applied to the final mixtures.

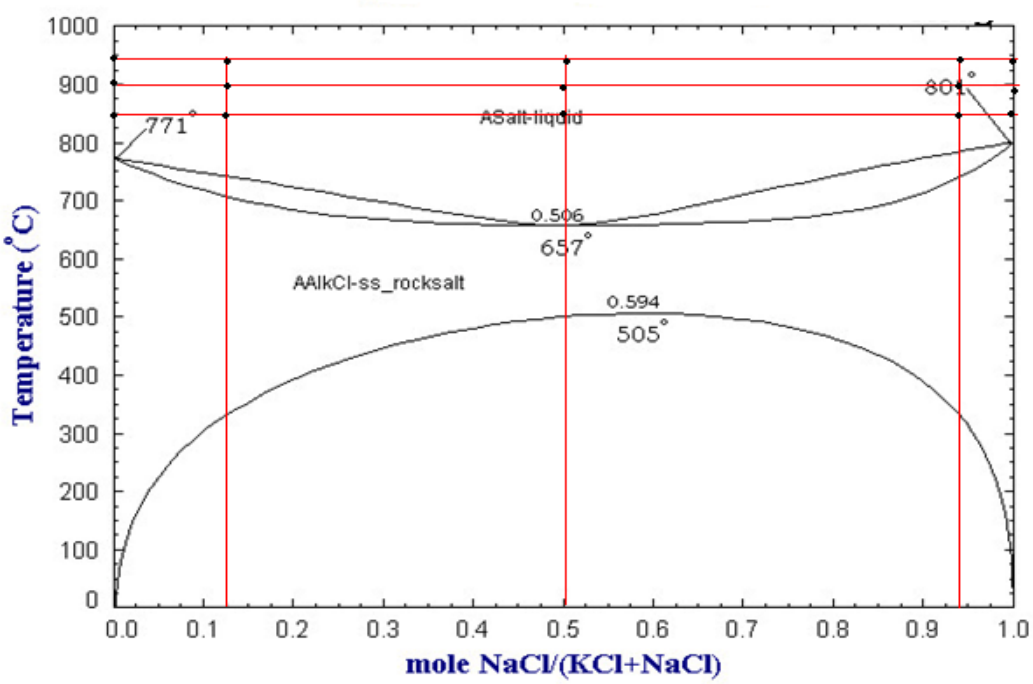

Figure 3.2 Binary phase diagram of NaCl and KCl including the flux compositions and calcination temperatures [70].

The average size of the platelets was measured by applying quantitative metallographic analysis on the scanning electron microscope (FE-SEM, FEI 430 NanoSEM, Oregon-USA) images.

3.2.3. Fabrication of BaHF-Polymer Matrix Electromagnetic (EM) Wave Absorbing Composites

EM wave absorbing composites composed of the synthesized BaHF powders as the filler materials and PS as the polymer matrix were fabricated by tape casting. BaHF powders synthesized by mixed oxide method or BaHF platelets synthesized by molten salt synthesis method were added to PS solutions to form dispersion to be casted.

3.2.3.1 BaHF Powder-Polymer Matrix Composite Production

BaHF powders synthesized by mixed oxide method were used as the inorganic filler of the EM wave absorbing composites. In the fabrication procedure, 30 ml of PS solution, composed of 65 wt% chloroform and 35 wt% PS in granular form, was mixed with 10, 20, and 30 wt% BaHF powders. The mixtures were put in a mixer and homogenized at 2000 rpm for 5 min. Obtained solution was tape casted with a thickness of 50 µm. Tapes were dried for 24 h. 6.5 x 6.5 cm squares were cut from the dried tapes.

In order to investigate the effect of texture on the EM wave absorption properties of the composites, the rest of the tapes were obtained without tape casting process. For that, 20 ml of PS solution was mixed with 10, 20, and 30 wt% BaHF powders, and homogenized at 2000 rpm for 5 min using a planetary centrifugal homogenizing mixer (Thinky ARE-310, Tokyo, Japan). Obtained solution was poured directly on a previously cleaned glass surface and dried for 24 h in ambient atmosphere. Square shaped specimens of size 6.5 x 6.5 cm were cut from the dried part.

5 square shaped individual specimens were stacked on top of each other to form the 5-layered BaHF powder-PS matrix composite. The thickness of the 5-layered composites was 250 μm.

3.2.3.2 BaHF Platelet-Polymer Matrix Composite Production

BaHF platelets synthesized by molten salt synthesis method were used to fabricate EM wave absorbing composites. As mentioned earlier, BaHF platelets were synthesized in five different flux compositions of 100 wt% NaCl, 90 wt% NaCl-10 wt% KCl, 44 wt% NaCl-56 wt% KCl, 10 wt% NaCl-90 wt% KCl, and 100 wt% KCl.

For the fabrication of the composites, 30 ml of PS solution, composed of 65 wt% chloroform and 35 wt% PS in granular form, was mixed with 30 wt% BaHF platelets synthesized in 5 different flux compositions.

These mixtures were put in the previously mentioned planetary centrifugal homogenizing mixer and homogenized at 2000 rpm for 5 min. Obtained dispersion was tape cast on a glass surface with a thickness of 50 μm. Tapes were dried in ambient air at 23 ºC for 24 h. Square shaped specimens of size 6.5 x 6.5 cm were cut from the dried tape.

In order to investigate the effect of texture on the EM wave absorption properties of the BaHF platelet-PS matrix composites, control samples were prepared by casting (without tape casting). 20 ml of PS solution was mixed with 30 wt% BaHF platelets synthesized in 100 wt% NaCl flux composition. This mixture was similarly homogenized at 2000 rpm for 5 min. The obtained solution was poured directly to a glass surface and dried for 24 h under identical ambient conditions. Square shaped specimens of size 6.5 x 6.5 cm were cut from the dried as-cast composite.

2 square shaped specimens were placed on top of each other to prepare a 2-layered BaHF platelet-PS matrix composite. The thickness of the 2-layered composite was ~100 μm.

3.2.3.3 BaHF Platelet and Graphite Flake or Nickel Flake-Polymer Matrix Composite Production

In order to improve the EM wave absorption properties of BaHF platelet containing composites, BaHF platelet and graphite flake or nickel flake-polymer matrix composites were prepared. For this purpose, 30 ml of PC solution, composed of 62 wt% chloroform and 38 wt% PC in granular form, was mixed with 3 g of BaHF platelet and 1 g of graphite flake (natural, -325 mesh, 99.8 %, metals basis-Alfa Aesar). In the case of the nickel flake containing composites, 30 ml of the above mentioned PC solution was mixed with 3 g BaHF platelets and 1 g nickel flake (-325 mesh, 0.37 micrometer thick, typically 99.8 %, metals basis-Alfa Aesar).

The mixtures were mixed and homogenized at 2000 rpm for 5 min. Obtained dispersions were tape casted with a thickness of 50 μm. Tapes were dried in ambient air at 23 ºC for 24 h. Square shaped specimens of size 6.5 x 6.5 cm were cut from the dried tapes.

Individual square shaped specimens were stacked on top of each other to form multilayered BaHF platelet and graphite flake or nickel flake-pc matrix composites. The effect of number of layers on the EM wave absorption properties of BaHF platelet and graphite flake or nickel flake-PC matrix multilayered composites were investigated in 18-40 GHz range.

3.3. Characterization

3.3.1. Microstructural Characterization

The sizes and morphologies of BaHF powders, BaHF platelets, graphite flakes and nickel flakes were examined by using scanning electron microscope (FE-SEM, FEI 430 NanoSEM, Oregon-USA). No metallographic preparation or coating was done to observe the samples in the microscope. Low accelerating voltages in the range of 5-10 kV was sufficient for the examinations since there was no coating.

Polished surfaces of the BaHF and Graphite or Ni flake containing polymer matrix composites were investigated by optical microscope. OLYMPUS PME3-F200 transmitted light metallurgical microscope was utilized both in bright-field and dark-field illumination modes for the observations of the BaHF/PS, BaHF/Ni-PC and BaHF/Graphite-PC composites.

3.3.2. Phase Analysis

X-Ray diffraction (XRD) technique was used to determine the phase content of the obtained powders and platelets. Rigaku D/MAX2200/ PC with Cu K_{α} source having $K_{\alpha 1}$=1.54056 Å and $K_{\alpha 2}$=1.5444 Å wavelengths was utilized in the 2θ range of 15º to 80º with a scanning rate of 2º/min. Quantitative XRD analyses were applied to the solid residues obtained from the flux compositions of 100 wt% NaCl, 90 wt% NaCl–10 wt% KCl, 44 wt% NaCl–56 wt% KCl (1:1 mol), 90 wt% KCl–10 wt% NaCl and 100 wt% KCl by using the software of Rigaku D/MAX2200/ PC. In this analysis the “Peak Fitting Approach” was utilized. Fitting of full X-Ray diffraction (XRD) patterns is an effective method for quantifying abundances during X-Ray diffraction analyses.

The basis of the method is that the observed diffraction pattern being the sum of the individual phases that the sample is composed of. By adding corundum (being a crystalline form of aluminum oxide with traces of iron, titanium and chromium) as an internal standard to both the observed patterns and to those for individual pure phases (standards), all patterns can be normalized to an equivalent intensity based on the internal standard intensity.

In the full-pattern fitting method, least-squares minimization is used for fitting the sum of individual pure standard patterns to the observed pattern for the optimization of fitting. A perfect match being 100% of standard patterns to the observed pattern is obtained, since the amount of internal standard used in both standards and unknowns is the same.

Figure 3.3 shows the data for a reaction product of heat-treated serpentine ($Mg_3(OH)_4(Si_3O_5)$) reacted in an autoclave at 200°C under high CO_2 pressure.

The observed pattern (with 20% corundum internal standard added) can be readily fit using measured standard patterns (also with 20% corundum internal standard added) of the meta-serpentine ($Mg_3Si_2O_5(OH)_4$), opal ($SiO_2 \bullet 1.5(H_2O)$), chlorite ($Mg_6Si_4O_{10}(OH)_8$), lizardite ($Mg_3Si_2O_5(OH)_4$ and magnesite ($MgCO_3$) reaction products. The difference pattern shows a very good fit with an unconstrained total of 99.5 wt% [71].

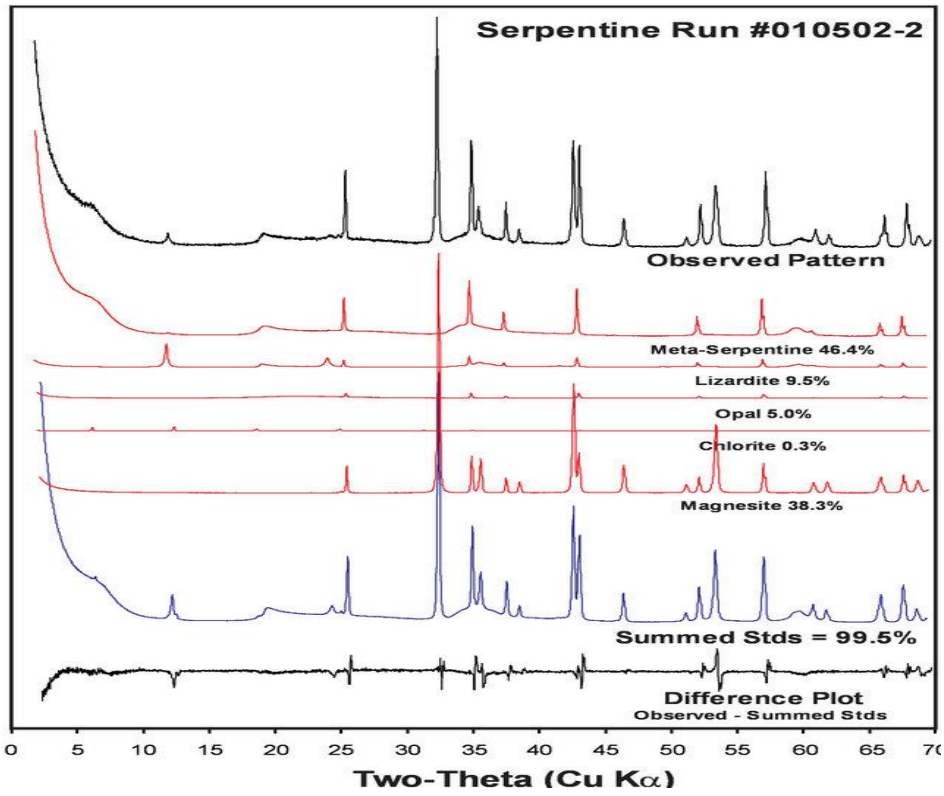

Figure 3.3 Full-pattern fitting analysis of an autoclaved and heat-treated serpentine [71].

3.3.3. Magnetic Characterization

Magnetic behavior of the synthesized BaHF powders and platelets were investigated via magnetic hysteresis curves obtained using vibrating sample magnetometer (VSM) (Cryogenic Limited PPMS, London- UK) at 300 K. B-H curves of the samples were obtained via vibrating sample magnetometer at external magnetic field values between 10000 and 10000 Oersteds applied where applied external magnetic fields were changing between $\mp 0.2\ T$.

VSM measurements were conducted on samples with powder form. Consequently, hysteresis loss and saturation magnetization were determined for the samples obtained by different processing parameters.

3.3.4. Electrical Conductivity Measurement

The electrical conductivities of BaHF/graphite and BaHF/Ni polymer matrix composites were measured using Jandel universal 4-point probe measurement system an example of which is schematically illustrated in Figure 3.4. Current is applied to the sample by the two end probes and voltage taken from the two middle probes is detected. By using the current and voltage values, sheet resistance and bulk resistivity of the samples were measured. For low resistivity materials (100 Ω-1 kΩ) 1-5 mA was applied while for high resistivity materials (1 kΩ-10 kΩ) applied current was 10 µA-0.1 mA.

The sheet resistance, R_S, of the composite tapes was determined using the following equation [72]:

$$R_S = \rho * V/I \qquad (\Omega/sq) \qquad (3.1)$$

where R_S is in per square, voltage V in mV and current I in mA where ρ is the geometric factor of the thin films or wafers being typically 4.5324.

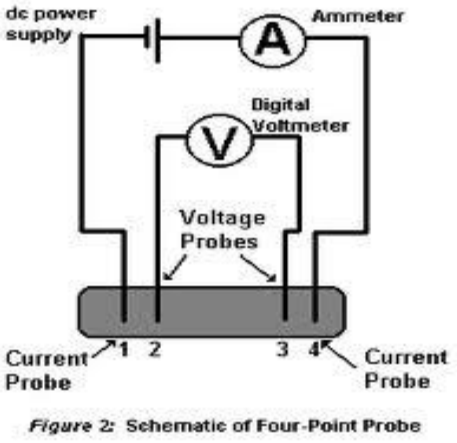

Figure 3.4 Four-Point probe measurement system [73].

3.3.5. Electromagnetic Characterization

Electromagnetic (EM) characterization of the BaHF composites in 18-40 GHz range was conducted using free-space method. Free-space method is a technique to characterize complex electromagnetic properties and EM wave reflection– transmission behavior of a media with certain thickness. This particular method has been chosen considering the advantages it provides such as applicability on inhomogeneous and/or anisotropic media [74]. Free-space measurement system consisting of two horn antennas and polymeric lenses facing each other is illustrated in Figure 3.5. Power generated by the network analyzer transferred via coaxial cables and power waves are emitted by antennas. Condensing lenses focus emitted wave to an area on the sample surface. Reflected and transmitted waves are collected and evaluated by network analyzer. In free-space method, electromagnetic properties of the content between the two antennas are characterized on the basis of electromagnetic circuit theory. Impedance/admittance against EM wave passage is measured within the spacing present between the two antennas.

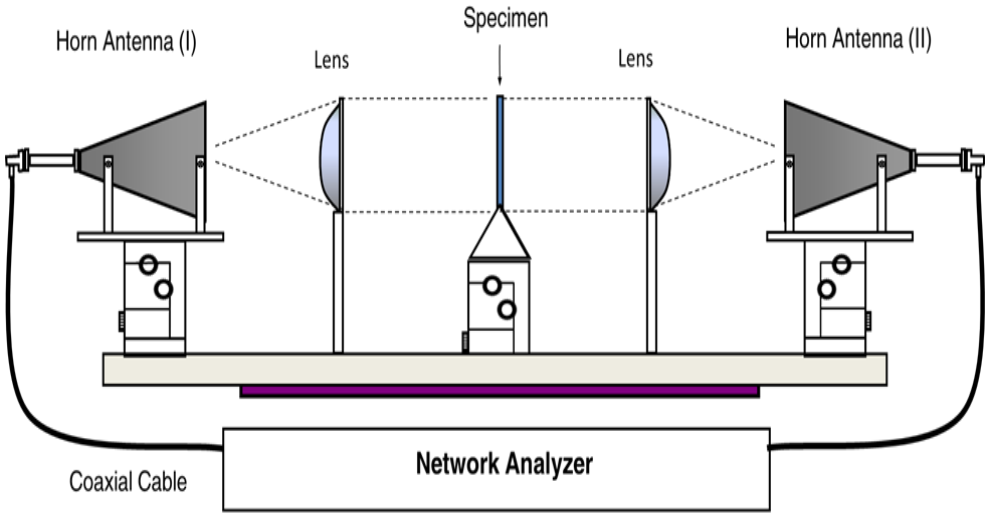

Figure 3.5 Set up of "Free-space method."

Waves reflected from the specimen surface as well as the ones transmitted through the specimen are collected and evaluated by the network analyzer (Anritsu 37269E, Vector Network Analyzer, 40 MHz-40 GHz, Anritsu Company, Morgan Hill CA, USA) in 18-40 GHz frequency range. Reflection (R_{dB}) loss and transmission loss (T_{dB}) values are recorded in terms of dB for different composite specimen sets. Reflection loss and transmission loss are indications of the ratio of the power reflected (P_R) or power transmitted (P_T) to total power supplied by the system (P_0) as given in the following two equations. Ratio of the power neither reflected nor transmitted is absorbed by the composite samples (% EM Wave Absorption) which can be determined by Equation 3.4 based on the principle of energy conservation.

$$R_{dB} = 10 \log \frac{P_R}{P_0} \tag{3.2}$$

$$\mathrm{T_{dB}} = 10 \log \frac{\mathrm{P_T}}{\mathrm{P_0}} \tag{3.3}$$

$$\%\ \text{EM Wave Absorption} = \ 1 - \ 10^{\mathrm{RdB}\ 10} - 10^{\mathrm{TdB}\ 10} \ \times 100 \tag{3.4}$$

During study, TRL calibration of the system is done prior to free-space measurements. After calibration, samples are placed into measurement opening at the center of the distance between the two horn antennas.

CHAPTER 4

4. RESULTS AND DISCUSSION

4.1. XRD and SEM Analyses of Powders Synthesized by Mixed Oxide Method

X-ray diffraction method was used to identify the phases present and to make quantitative phase analysis of the powders synthesized by mixed oxide method. Figure 4.1 shows the XRD pattern of the BaHF powders revealing the presence of BaHF as the only phase.

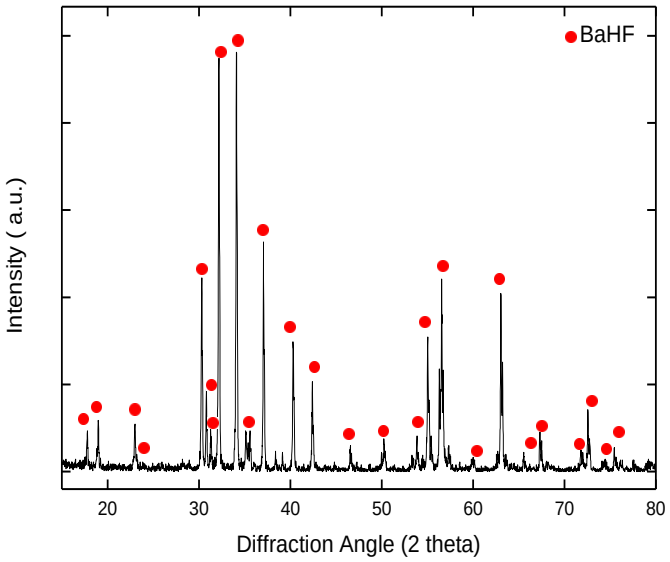

Figure 4.1 X-ray diffraction pattern of BaHF powders prepared by mixed oxide method (JCPDS-ICDD card no. BaHF 43-0002).

BaHF powders prepared by mixed oxide method can be seen in the SEM image provided in Figure 4.2. The particles seem to be hexagonal in shape. The average length of the powders has been determined to be between 500 ± 100 nm.

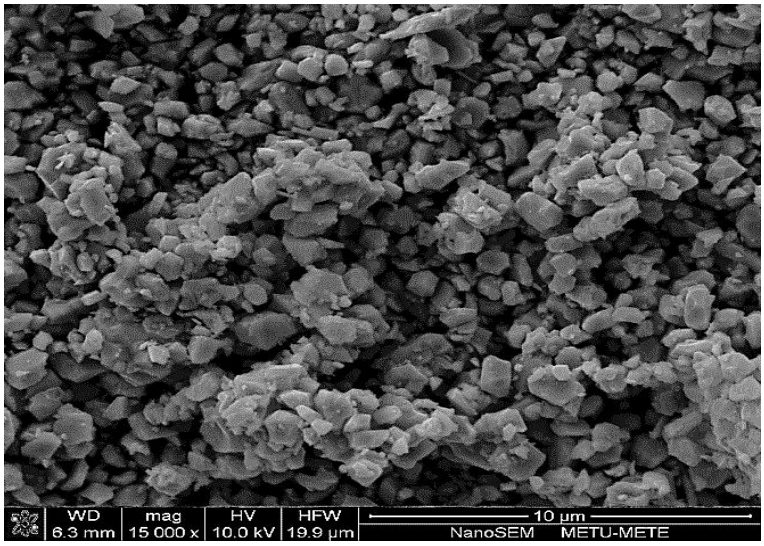

Figure 4.2 SEM image of BaHF powders prepared by mixed oxide method.

4.2. SEM and XRD Analyses of Platelets Synthesized by Molten Salt Synthesis

The platelets were synthesized in molten salt in order to be used in a further study for the fabrication of BaHF-polymer matrix electromagnetic wave absorbing composites utilizing tape casting technique. Thus, the largest possible platelet radius with high aspect ratio was desired. Calcination time, temperature, flux type and composition were investigated systematically in order to determine the optimum condition to achieve maximum possible platelet size.

Figure 4.3 shows the platelet size distribution as a function of flux composition for varying calcination durations and temperatures. It is observed that under all conditions platelet size in KCl flux is the smallest.

With the increase in the NaCl flux content, platelet size increases. However, after a certain concentration approaching the equi-molar flux composition, platelet size starts to decrease. It should be noted that platelet size in NaCl flux was larger than that in KCl for all calcination temperatures and durations applied. This demonstrates the lower apparent activation energy for platelet growth in NaCl rich fluxes. As a result, for the same calcination temperatures and durations, the apparent activation energy for platelet growth in NaCl flux should be lower than that in the KCl flux. Compared to other temperatures, platelet size at 900 °C was the largest for most of the compositions, especially for 2 h calcination duration. For this reason, morphology studies using SEM, quantitative phase analysis using XRD, magnetic characterization using VSM and characterization of the electromagnetic wave absorption properties of the resulting composites using free-space method with the network analyzer were concentrated on the BaHF platelets calcined at 900 °C for 2 h.

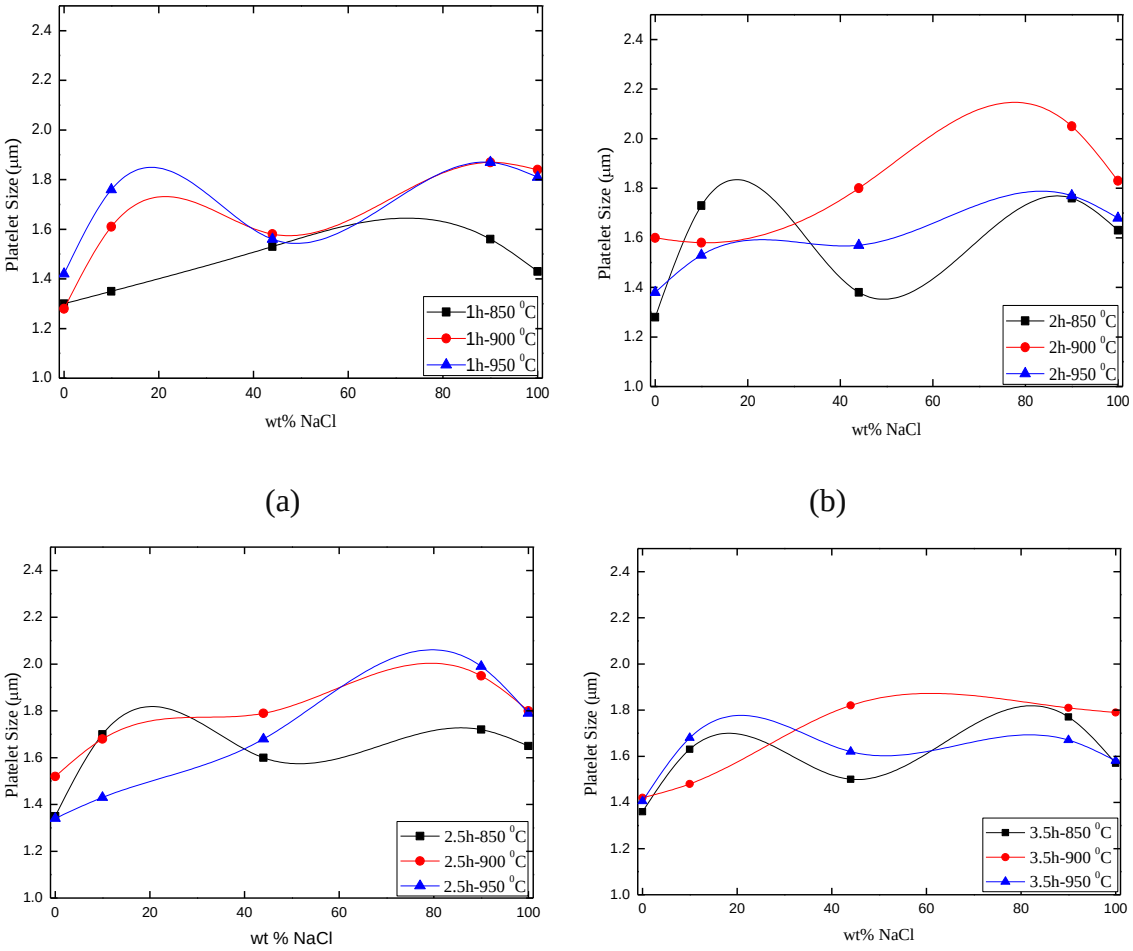

Figure 4.3 Platelet size as a function of flux composition at 850, 900 and 950 °C for (a) 1 h, (b) 2 h, (c) 2.5 h and (d) 3.5 h of calcination. Fit to the data point are for visual aid.

SEM images in Figure 4.4 illustrate both the morphologies and the platelet sizes at 900 °C for 2 h calcination of BaHF platelets synthesized in molten salt.

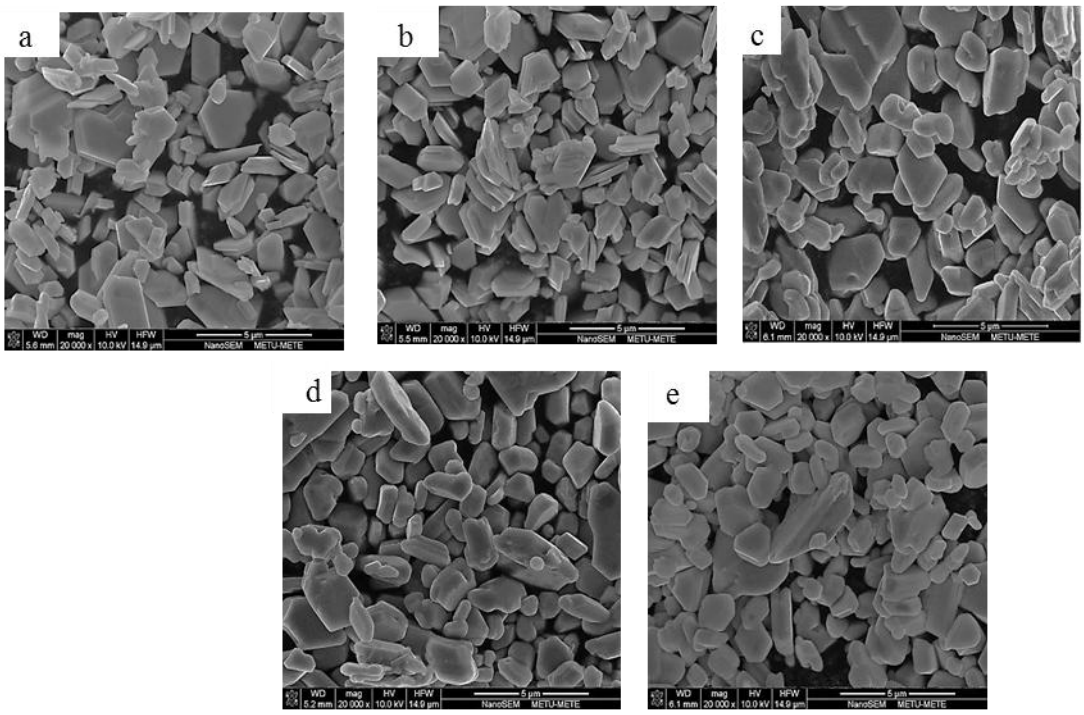

Figure 4.4 SEM images of BaHF platelets calcined in (a) 100 wt% KCl, (b) 90 wt% KCl-10 wt% NaCl, (c) 44 wt% NaCl- 56 wt% KCl, (d) 90 wt% NaCl- 10 wt% KCl, and (e) 100 wt% NaCl at 900 °C for 2 h.

Regarding the morphology of the BaHF platelets, in the case of the synthesis at 900 °C in NaCl flux, corners of the platelets became rounder (Figure 4.4 (e)). This is speculated to be caused by the selective desorption from the corners as a result of curvature dependent chemical potential change around the sharp corners of the platelets in the molten NaCl flux. In the case of platelet synthesis in KCl flux, either no desorption occurred or desorption occurred homogenously on all the surfaces and corners of the platelets so that platelet shape with sharp corners was preserved (Figure 4.4 (a)). The aspect ratios of the platelets was determined to be approximately 3 to 4 for all calcination conditions.

Figures 4.5-4.9 show the phase content of the BaHF platelets synthesized by molten salt synthesis method at 900 °C for 2 h with different flux types and compositions. In all of the XRD patterns presence of some amount of remaining Fe_2O_3 phase can be observed. The amount of Fe_2O_3 phase is decreasing as the content of NaCl in the flux increases.

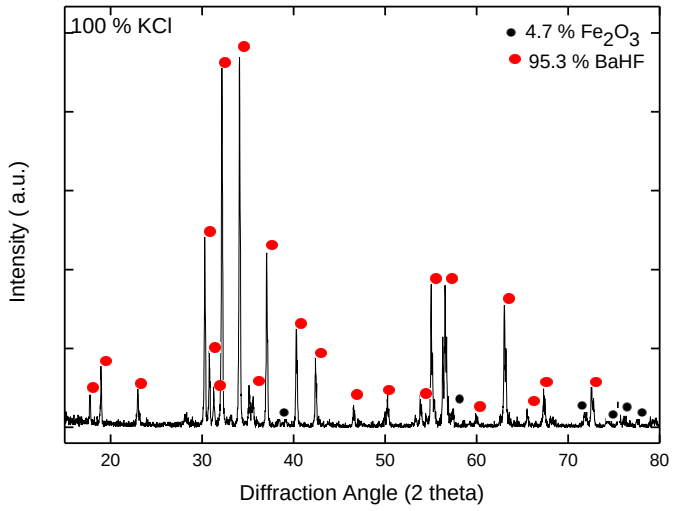

Figure 4.5 X-Ray diffraction pattern of BaHF platelets synthesized in 100 wt% KCl flux composition.

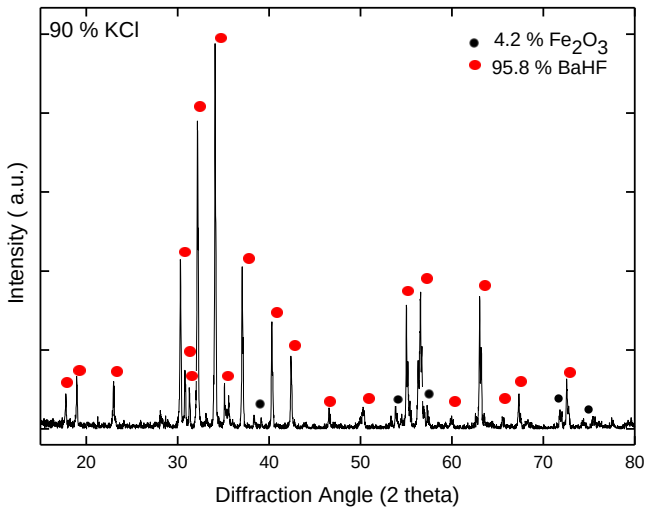

Figure 4.6 X-Ray diffraction pattern of BaHF platelets synthesized in 90 wt% KCl- 10 wt% NaCl flux composition.

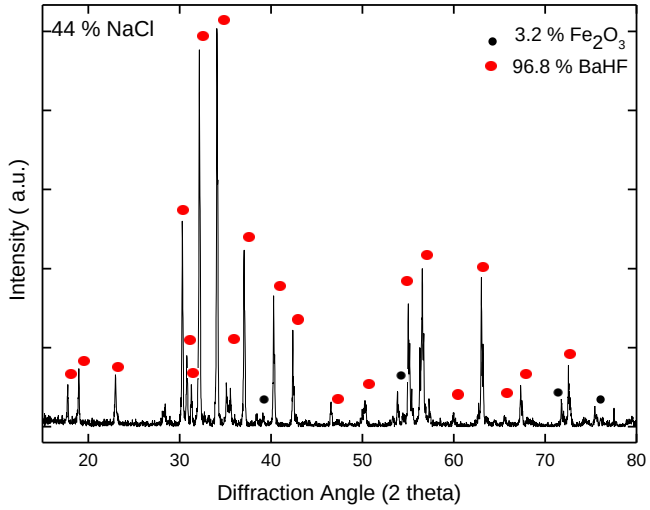

Figure 4.7 X-Ray diffraction pattern of BaHF platelets synthesized in 44 wt% NaCl- 56 wt% KCl flux composition.

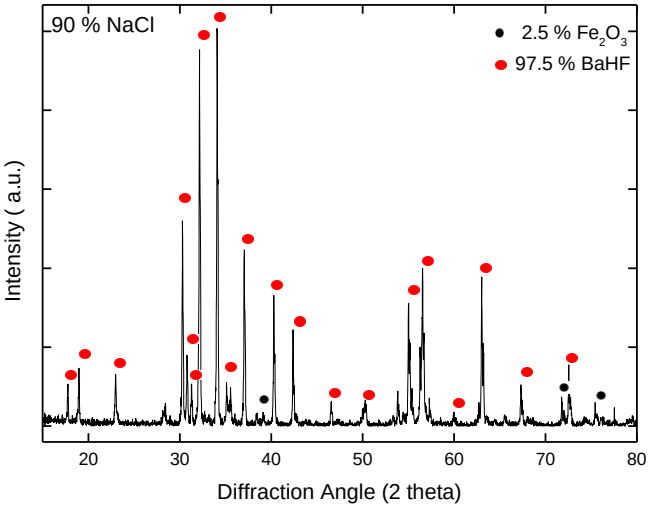

Figure 4.8 X-Ray diffraction pattern of BaHF platelets synthesized in 90 wt% NaCl- 10 wt% KCl flux composition.

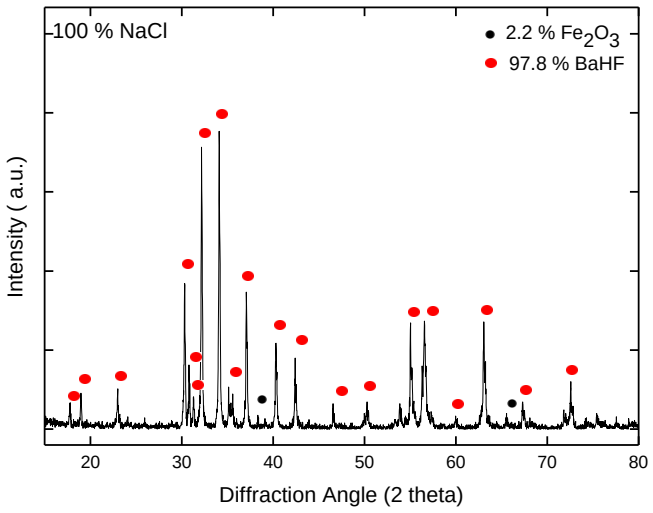

Figure 4.9 X-Ray diffraction pattern of BaHF platelets synthesized in 100 wt% NaCl flux composition.

Figure 4.10 shows the amount of BaHF phase formed during calcination at 900 ºC for 2 h as a function of flux composition which was determined using quantitative XRD analysis.

It is obvious that formation of BaHF phase within the system is the lowest when synthesis has been done in 100 wt% KCl flux. With the increase in the NaCl content, the amount of BaHF phase increases gradually up to 97.8 wt% at 100 wt% NaCl flux composition.

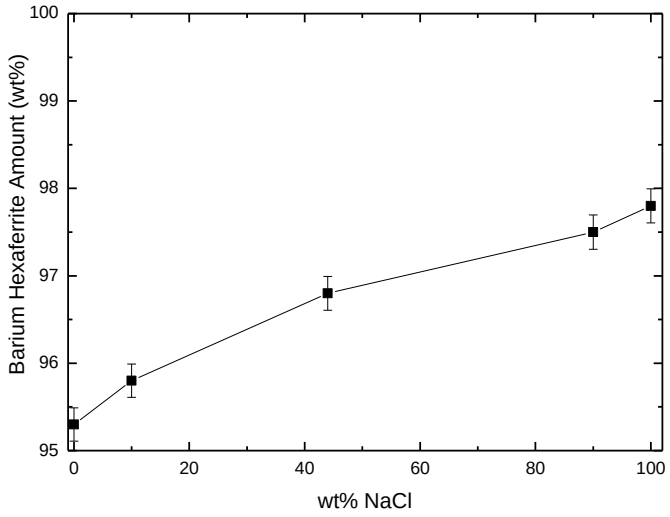

Figure 4.10 Quantitative XRD analysis of the platelets calcined at 900 ºC for 2 h in varying flux compositions.

4.3. Magnetic Measurement Results of BaHF Powders and Platelets

The magnetic response of the BaHF powders synthesized by mixed oxide method has been determined using VSM at 300K (See Figure 4.11). M–H curve of the BaHF powder exhibits a clear hysteresis behavior for the magnetization under the applied magnetic field. When the applied magnetic field is around 10 kOe, the magnetization saturates. The saturation magnetization value reaches to 58.1 emu/g.

Hysteresis curves were obtained at 300K for the BaHF platelets synthesized by molten salt synthesis method at 900 °C for 2 h in 100 wt% KCl, 10 wt% NaCl, 44 wt% NaCl, 90 wt% NaCl and 100 wt% NaCl (See Figure 4.12). BaHF powders exhibit a clear hysteresis behavior for the magnetization under the applied magnetic field as seen in Figure 4.12. When the applied magnetic field is around 10 kOe, the magnetization saturates. As the NaCl content in the molten flux increases, the area under the hysteresis curve increases, and the ceramic reveals a stronger hard magnetic behavior.

The saturation magnetization (M_s), remanent magnetization (M_r), squareness ratio (M_r/M_s) and the coercive field (H_c) of the BaHF platelets obtained from figures 4.11 and 4.12 are given in table 4.1.

Complete conversion of the initial oxide materials to BaHF upon mixed oxide synthesis improved the saturation magnetization value of BaHF powders. Highest magnetization was obtained for the BaHF powders processed by the mixed oxide method, which was 58.1 emu/g as indicated in Table 4.1.

In the case of BaHF platelets synthesized by the molten salt method, as the NaCl content increases, there is an increase in the BaHF formation that improves the hard magnetic behavior of the ceramics.

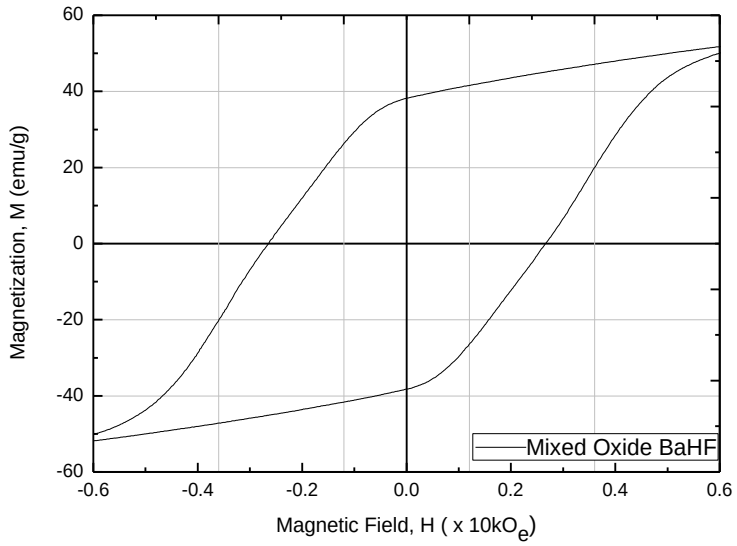

Figure 4.11 300K hysteresis curve of the BaHF powder synthesized by the mixed oxide method.

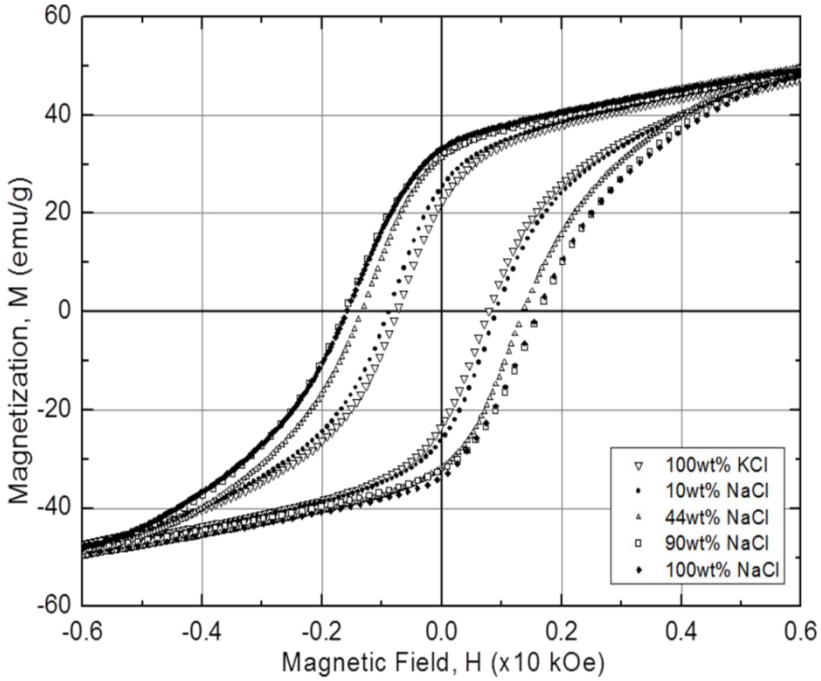

Figure 4.12 300K hysteresis curves of BaHF platelets synthesized in 100 wt% KCl, 90 wt% KCl, 44 wt% NaCl, 90 wt% NaCl and 100 wt% NaCl.

Table 4.1. Magnetic properties of BaHF powders and platelets synthesized by mixed oxide method and by molten salt synthesis method in five different molten flux compositions.

Flux Composition (wt%)	BaHF Amount (wt%)	H_c(Oe)	M_r(emu/g)	M_s(emu/g)	M_r/ M_s
Mixed Oxide	100	2660	38.15	58.1	0.65
100 wt% KCl	95.3	753	21.9	55.0	0.40
90 wt% KCl-10 wt% NaCl	95.8	838	25.0	54.3	0.45
44 wt% NaCl	96.8	1380	31.4	56.5	0.55
90 wt% NaCl	97.5	1600	32.0	55.2	0.58
100 wt% NaCl	97.8	1600	33.2	55.6	0.59

Although magnetic saturation values change around 55 emu/g for all flux compositions, the highest saturation value of 56.5 emu/g was obtained in the case of 44 wt% NaCl composition. On the other hand, the highest coercivity of 1600 Oe was obtained for 90 wt% NaCl and 100 wt% NaCl compositions. It is clear that an increase in the NaCl content in the flux improves the BaHF conversion which in turn results in higher coercivity and remanant magnetization. High coercivity and remanant magnetization indicate the augmentation in the hard magnetic behavior of the synthesized ceramics.

BaHF powders synthesized by mixed oxide method have higher saturation magnetization than BaHF platelets synthesized by molten salt method. The reason for this is that, in mixed oxide method, higher amount of BaHF is produced and so all the magnetic dipoles in a solid piece are mutually aligned with the external field causing an increase in the saturation magnetization. The other reason is that, BaHF platelets have larger sizes than BaHF powders causing, multi-domain formation and the easy movement of the domain walls, therefore decreasing the coercivities.

For the BaHF platelets, as the NaCl content in the flux increases, the platelet average length increases, therefore the aspect ratio of the platelets increase and thus the coercivity is increased.

4.4. Morphology of Graphite and Nickel Flakes

The size and morphology of the graphite flakes used in the electromagnetic wave absorbing polymer matrix composites along with the synthesized BaHF powders were investigated using field emission type SEM. No metallographic surface preparation or coating was applied to observe the samples in the microscope. Low accelerating voltage in the range of 5-10 kV was utilized for the examinations. In the recorded images 10 flakes were chosen randomly and size measurements were conducted on these flakes and the average of the 10 measurements were reported.

According to the measurements the graphite flakes have hexagonal morphologies with average length of 20 μm and average thickness of 0.73 μm leading to an aspect ratio of 27.4. The Ni flakes have irregular morphology with average length of 15 μm and average thickness of 0.57 μm resulting in an aspect ratio of 26.3.

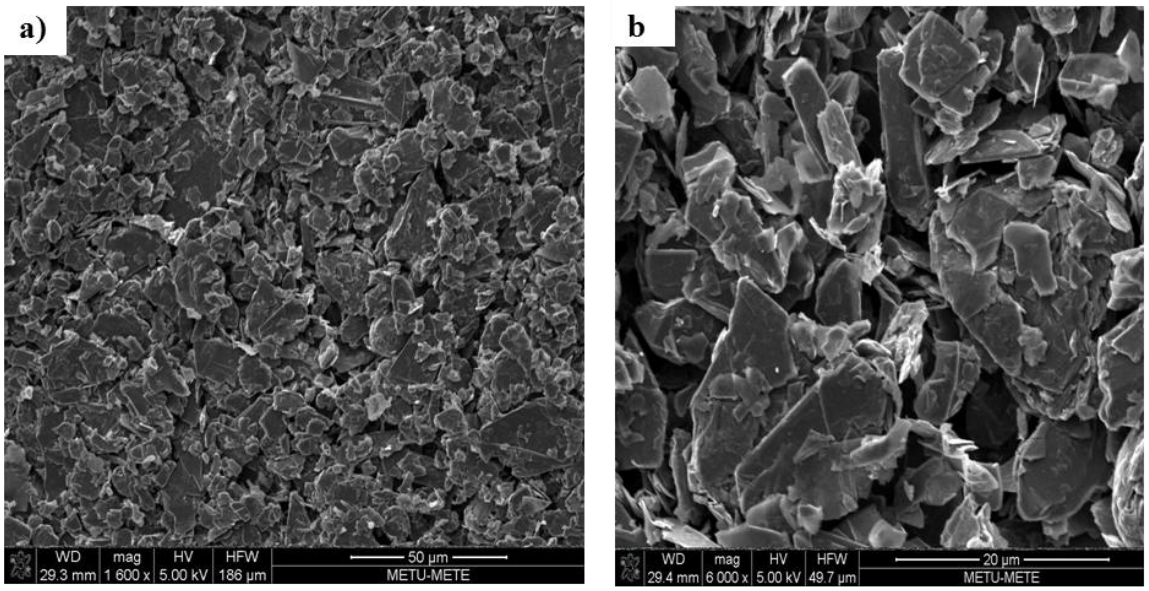

Figure 4.13 SEM images of graphite flakes at two different magnifications (a) 1600x, (b) 6000x.

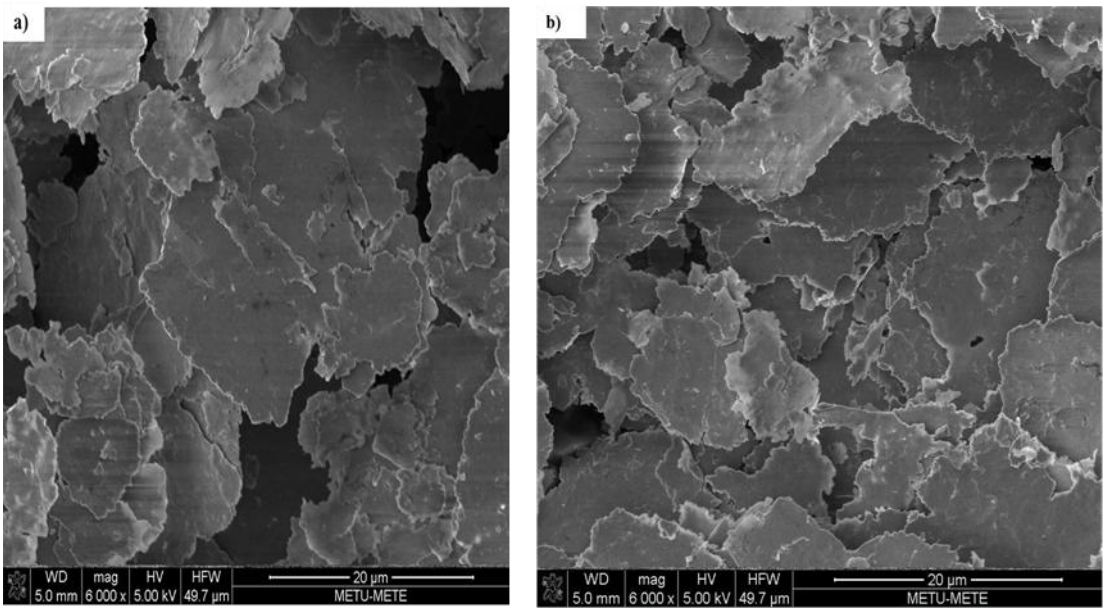

Figure 4.14 SEM images of Ni flakes at 6000x magnification at two different locations in the sample.

4.5. Microstructure of BaHF and Graphite or Ni Flake Containing Polymer Matrix Composites

4.5.1 BaHF Powder-PS Composites

Figure 4.15 a, b, c show the optical microscope images of tape cast PS matrix composites containing 10, 20 and 30 wt% BaHF powders. As the amount of BaHF in the composite increases, the surface coverage of the particles in the tapes seems to be increasing as expected. The least particle network formation and hence surface coverage is observed in the composite tape containing 10 wt% BaHF, which is evident from the bright, transparent regions in Figure 4.15 a. The highest amount of surface coverage was obtained in the composite tape containing 30 wt% BaHF as seen in Figure 4.15 c.

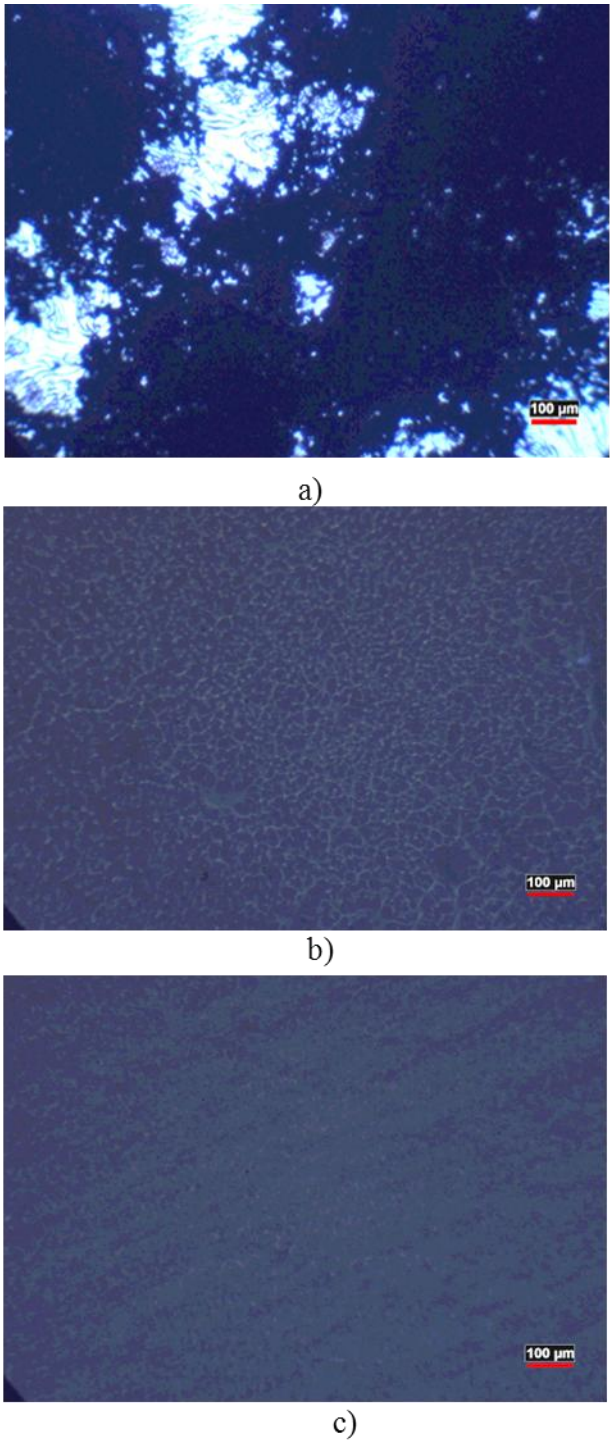

Figure 4.15 Optical microscope image of tape cast a) 10 wt% BaHF/PS composite b) 20 wt% BaHF/PS composite c) 30 wt% BaHF/PS composite (50x).

Figure 4.16 a, b and c show the optical microscope images of as-cast 10, 20 and 30 wt% BaHF powder containing PS matrix composites at higher magnification. Since composites are as-cast there is no particle alignment expected resulting in inhomogeneous particle distribution in the composite structures. It is observed that the BaHF particles are oriented randomly with fairly uniform distribution. Besides the morphology of the as-cast composites, as the content of BaHF in the composite increases, the particle coverage in the structure seems to be increasing. Similar to the case with the previously discussed tape-cast composites, the least particle network formation and hence surface coverage is observed in the composite containing 10 wt% BaHF, while the highest coverage is observed in 30 wt% BaHF containing composite.

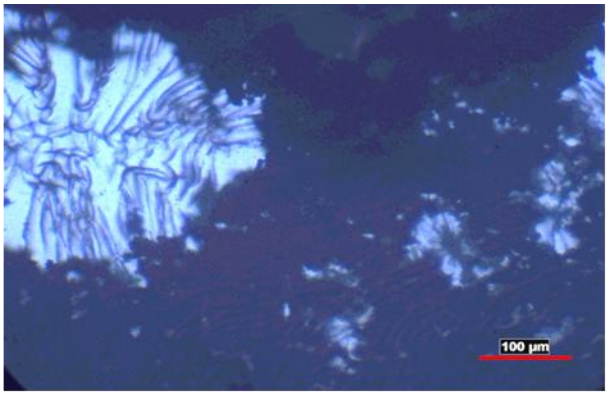

a)

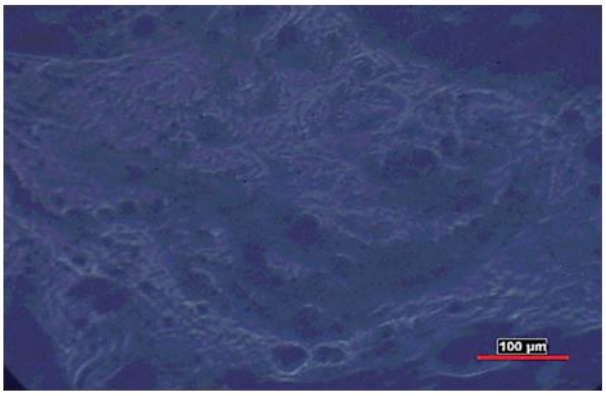

b)

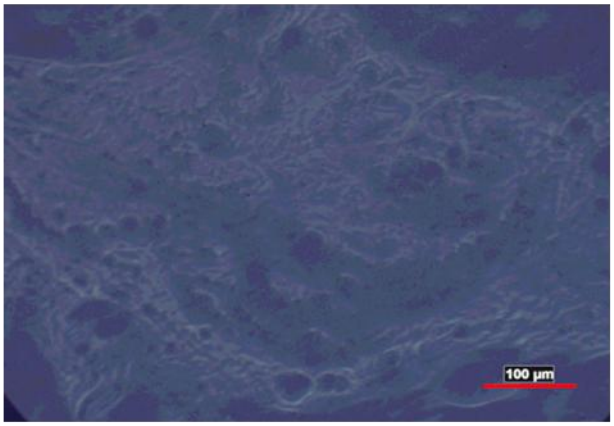

c)

Figure 4.16 Optical microscope image of as cast a) 10 wt% BaHF/PS composite b) 20 wt% BaHF/PS composite c) 30 wt% BaHF/PS composite (100x).

4.5.2 BaHF- Graphite Flake / PC Composites

The surfaces of the BaHF powder and graphite flake containing PC matrix composites were investigated using an inverted type metallurgical microscope at 500x magnification (See Figure 4.17). Regions designated by "**A"** in Figure 4.17 b) and d) are the graphite flakes distributed in the PC matrix, while the regions designated with "**B"** show the PC matrix containing BaHF powders.

Figure 4.17 show different locations on the surface of the same composite again at 500x magnification. The average size of graphite flakes measured as 20 μm is matching with the sizes of the regions shown as "A". The graphite flakes seems to be in contact with each other pointing out to the achievement of percolation in tape-cast polymer matrix composites containing graphite flakes.

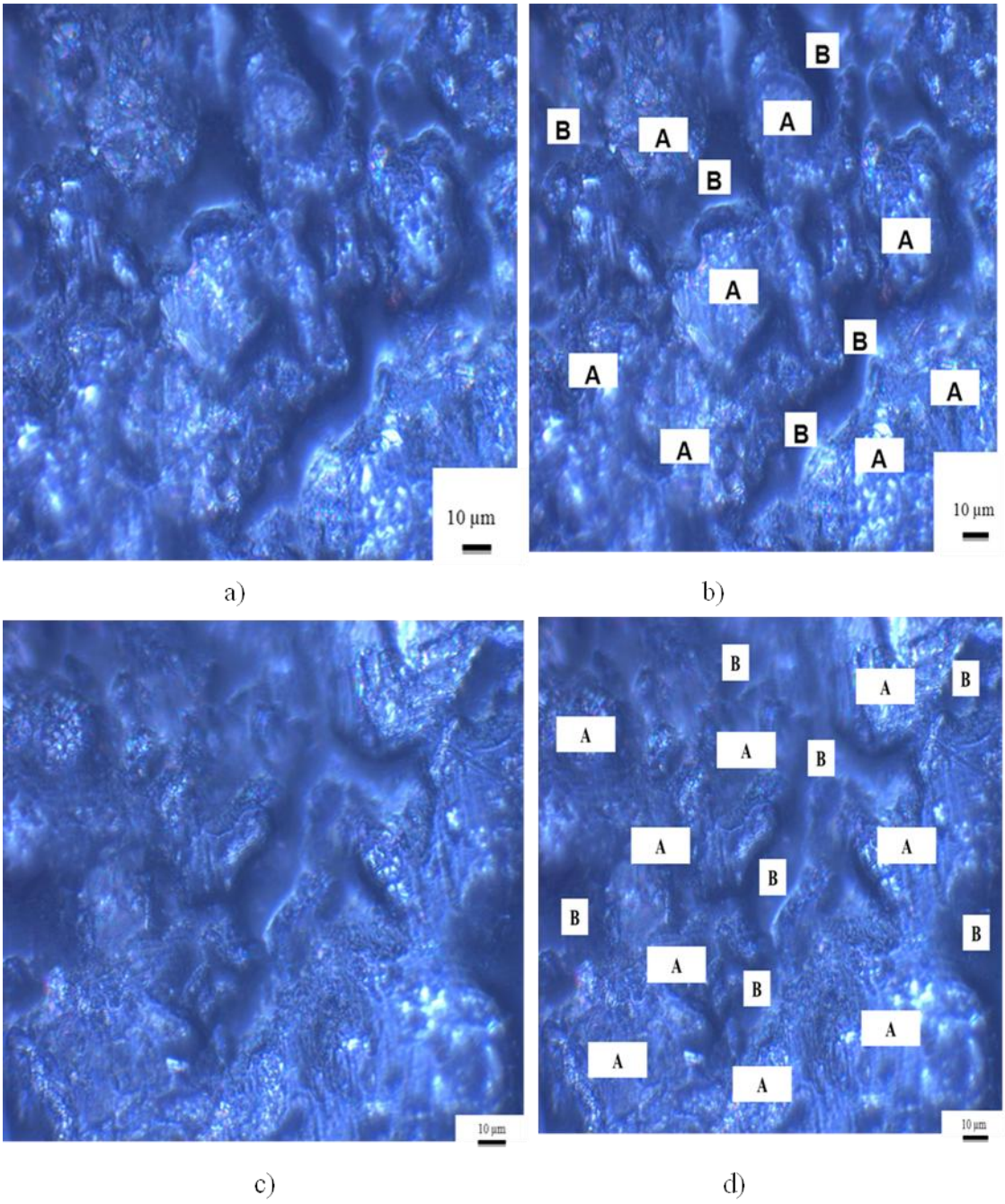

Figure 4.17 Optical microscope images of a-d) BaHF/Graphite-PC composites from different locations of the samples (500x).

4.5.3 BaHF- Nickel Flake / PC Composites

Similar to the previous case, surfaces of the BaHF powder and Ni flake containing PC matrix composites were investigated using the inverted type metallurgical microscope at 200x (See Figure 4.18 a-d)) and at 500x magnification (See Figures 4.18 e), f)). In Figures 4.18 b, d and f regions designated by **"A"** are the nickel flakes aligned parallel to the composite tape surface, while the ones shown as **"C"** are the Ni flake aligned vertical to the tape surface. The regions marked as **"B"** are the BaHF agglomerates. The average size of Ni flakes was measured as 15 μm, which is matching with the size of the regions shown as "B".

It is clear in Figure 4.18 that these Ni flake regions are not in contact with each other pointing out to the lack of percolation of Ni flakes in the tape-cast polymer matrix composites.

Even though network formation could have been achieved in graphite flake containing composites, this does not seem to be the case with Ni flake containing ones. This can be attributed to the difference in the rigidity of the two flakes.

The graphite flakes are much more rigid compared to the Ni flakes although they have comparable aspect ratios. Presence of two different flake orientations in the Ni flake containing composite tapes, namely horizontal and vertical, points out to the fact that Ni flakes fold or bend during tape casting hindering their effective alignment with their basal surfaces parallel to the tape surface. Consequently, Ni flakes cannot form a network structure in the composite tapes.

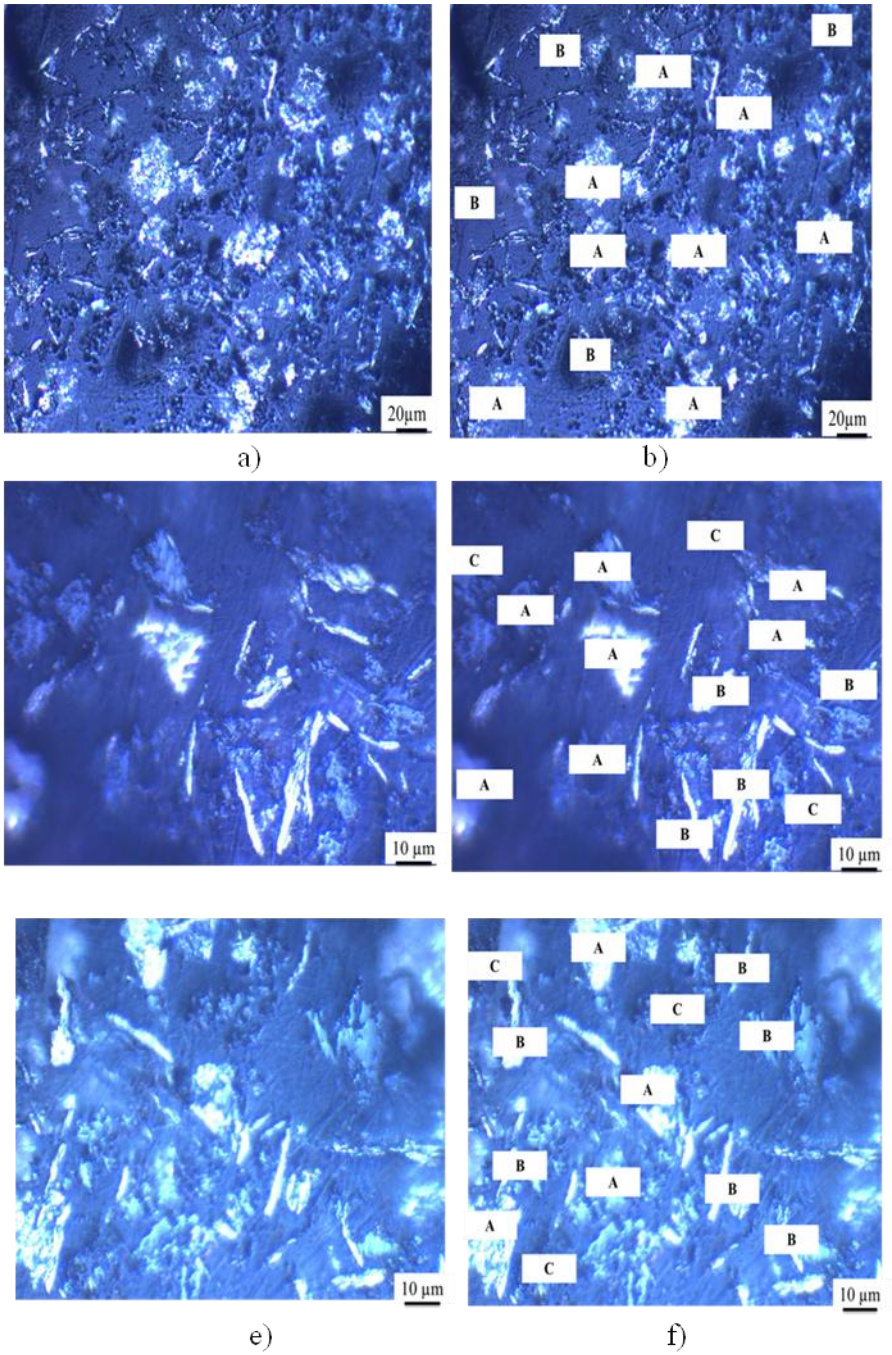

Figure 4.18 Optical microscope images of a-d) BaHF/Ni-PC Composite (200x), e), f) BaHF/Ni -PC Composite (500x).

4.5.4 Macroscopic Images of BaHF-Polymer matrix composites

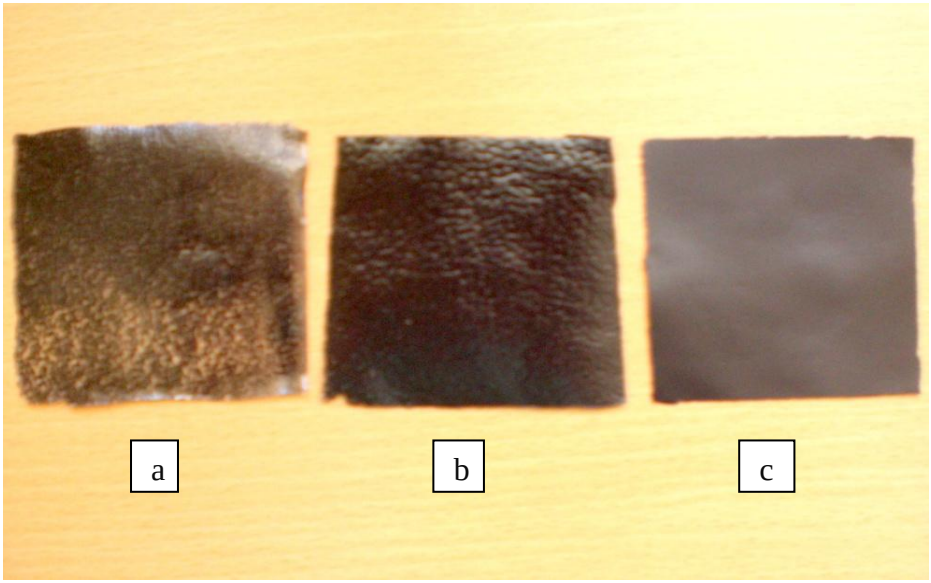

Figure 4.19 Macroscopic images of a) tape cast 10 wt% BaHF/PS composite b) tape cast 20 wt% BaHF/PS composite, c) tape cast 30 wt% BaHF/PS composite.

Figure 4.19 shows the macroscopic images of tape cast 10, 20 and 30 wt% BaHF/PS composites. As the BaHF content in the tape increases, the surface of the tape becomes denser.

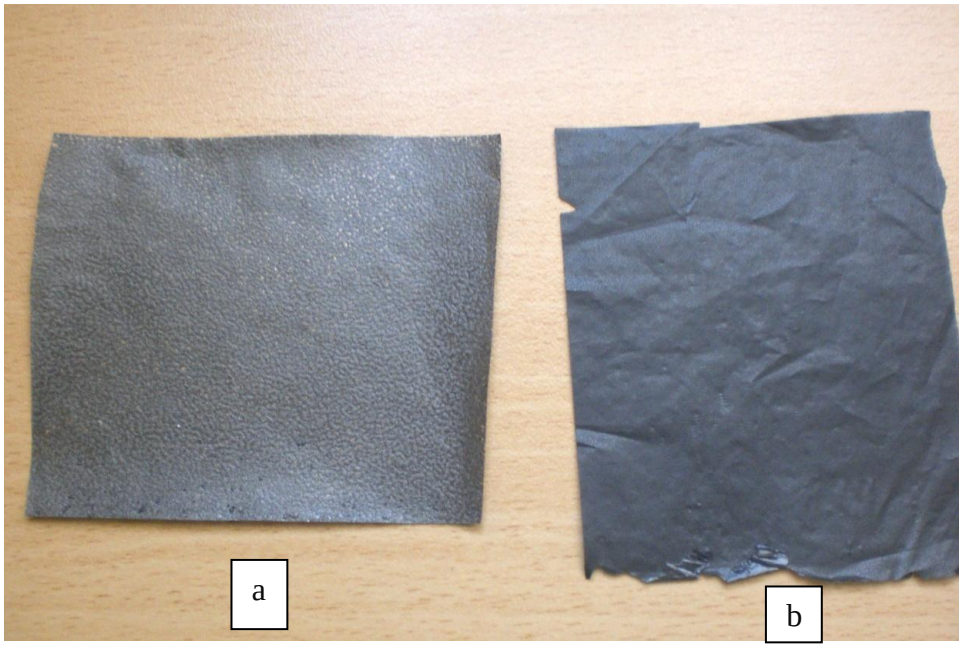

Figure 4.20 Macroscopic images of a) tape cast BaHF/Ni-PC composite b) tape cast BaHF/graphite-PC composite.

Figure 4.20 shows the macroscopic images of tape cast BaHF/Ni-PC composite and tape cast BaHF/graphite-PC composites.

4.6. Electrical Properties of Graphite or Ni Flake Containing Tape-Cast Composites

The sheet resistance (R_s) of graphite or Ni flake containing composites was measured by four point probe measurement method. Sheet resistance of the BaHF/graphite flake composite was determined to be 13.5 kΩ /sq. However, in the case of Ni flake containing composites electrical conduction could not be measured within the sensitivity of the above-mentioned four-point probe measurement setup.

Although Ni has a higher bulk electrical conductivity than graphite (conductivity of bulk nickel is 14.3 x 10^6 S/m [75], conductivity of bulk graphite is 2 to 3 x 10^5 S/m when electrical field is perpendicular to basal plane, 3.3 x 10^2 S/m when electrical field is parallel to basal plane [76]), electrical conduction in the Ni flake containing composites could not be achieved.

This can be attributed to the lack of network formation and hence percolation of Ni flakes as demonstrated in Figure 4.18.

As mentioned earlier, Ni flakes were not aligned well during tape casting due to lack of their rigidity hindering percolation in the composite tape structure. Because of this reason a measurable electrical conductivity was not detected by the used four point probe measurement setup in the Ni flake containing polymer matrix composites. On the contrary to this, as shown in Figure 4.17 graphite flakes can be aligned well by tape casting in the composite structure due to their superior rigidity. Consequently, graphite flakes with their basal surfaces aligned parallel to the surface of the composite tape come into contact with each other forming a network and providing the measured electrical conduction.

4.7. Electromagnetic Properties of BaHF Based Polymer Matrix Composites

4.7.1 BaHF Powder/PS Composites

In order to investigate the effect of BaHF amount on the EM wave reflection and transmission characteristics of BaHF/PS composites within 18-40 GHz frequency range, reflection and transmission loss of 10 wt%, 20 wt% and 30 wt% BaHF powder containing composites are presented in Figure 4.21. It is clear that as BaHF content in the PS matrix increases, reflection loss of the composite increases, which is evident from the increasing dB values pointing out to stronger reflection from the composite surface. This is something expected, since the EM waves incident to the composite surface encounter to more inorganic particles with increasing BaHF content leading to higher reflection.

Even though particle content dependence of the transmission loss of the composites is not that pronounced, still a slight decrease in transmission loss evident from the decreasing dB values pointing out to weaker transmission through the composite with increasing inorganic content can be observed. This is similarly expected, as more frequent interaction of EM waves with the increasing amount of particles hinders the passage of the EM waves through the material.

Electromagnetic wave absorption values of the composites calculated from the measured reflection and transmission losses based on the principle of conservation energy sample is given in Figure 4.22. It is clear from this figure that increasing BaHF particle content results in stronger EM wave absorption. This points out to the increasing lossy character of the composite with increasing BaHF content mainly based on the magnetic loss provided by the ferrimagnetic nature of the synthesized BaHF powders. EM wave absorption of the composite containing 30 wt% BaHF powder changes between 5 and 35 % being highest among the other two composites.

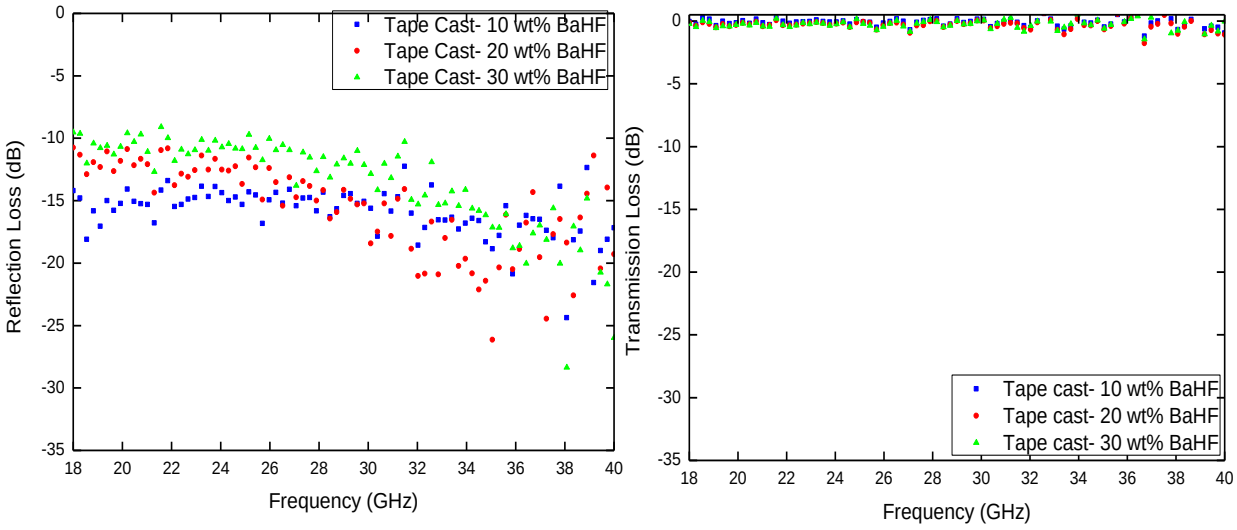

Figure 4.21 EM wave reflection and transmission losses of 10, 20, 30 wt% BaHF powder containing PS matrix tape-cast composites.

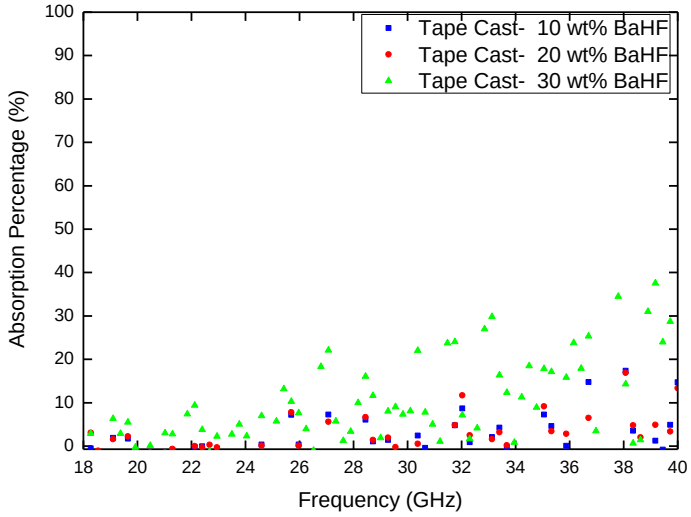

Figure 4.22 EM wave absorption of 10, 20, 30 wt% BaHF powder containing PS matrix tape-cast composites.

EM wave interaction characteristics of as-cast BaHF powder /PS composites were also investigated in order to determine the effect of processing method on their EM wave reflection, transmission and hence absorption properties.

As seen in Figure 4.23, similar to the above discussed case reflection loss increases and transmission loss decreases with increasing BaHF content in as-cast PS matrix composites. EM wave absorption of as-cast composites is shown in Figure 4.24. In the case of as-cast composites EM wave absorption changes between 5 and 25% independent of the BaHF content. Lower levels of EM wave absorption independent from the inorganic content in the as-cast composites reveals the positive effect of tape casting in the EM wave characteristics of BaHF containing composites resulting from the uniform particle arrangement it provides in the structure. However, the effect of tape casting on the EM wave absorption is not that pronounced, since in the case of the BaHF powders tape casting cannot provide any alignment and hence considerable change in the EM wave characteristics.

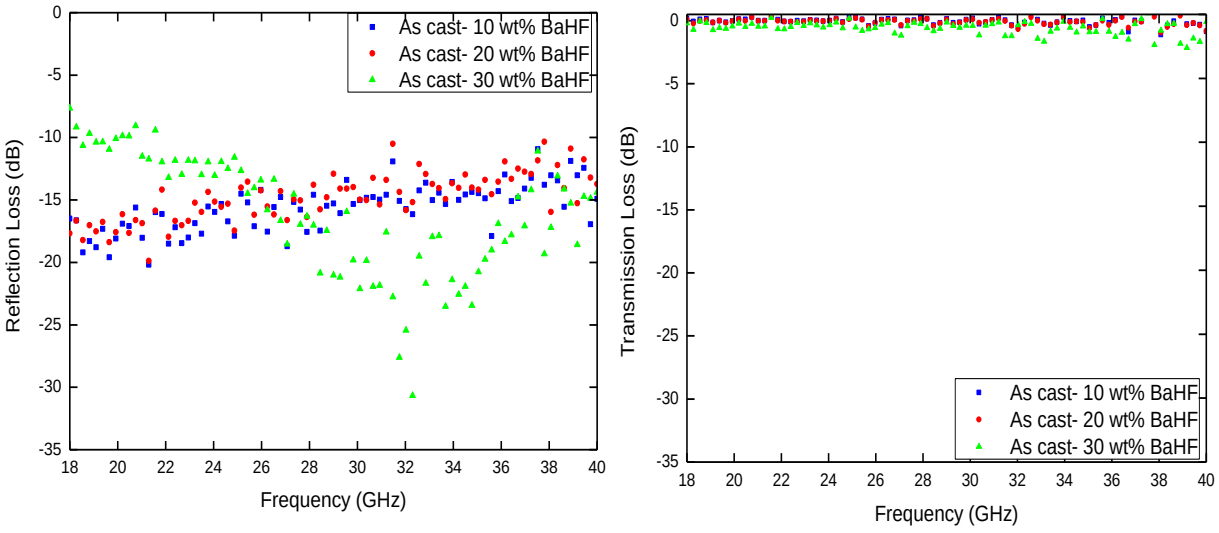

Figure 4.23 EM wave reflection and transmission losses of 10, 20, 30 wt% BaHF powder containing PS matrix as-cast composites.

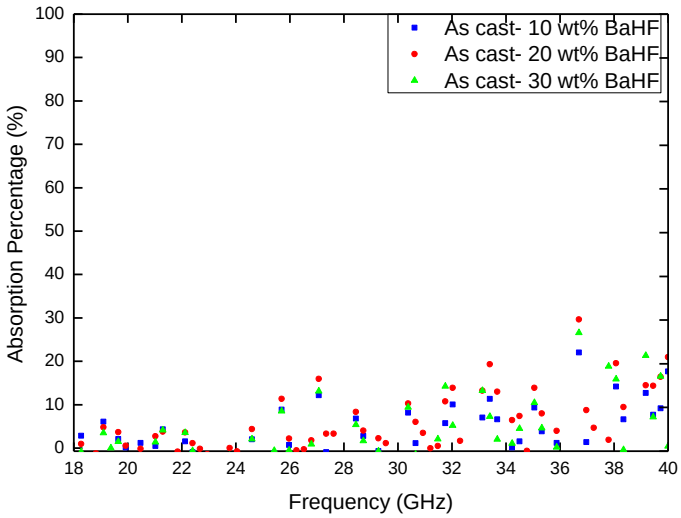

Figure 4.24 EM wave absorption of 10, 20, 30 wt% BaHF powder containing PS matrix as-cast composites.

4.7.2 BaHF Platelet/PS Composites

The effect of NaCl-KCl flux composition on the EM wave interaction characteristics has been examined. 5 different flux compositions were taken into consideration, namely 100 wt% KCl, 90 wt% KCl- 10 wt% NaCl, 56 wt% KCl-44 wt% NaCl, 90 wt% NaCl-10 wt% KCl and 100 wt% NaCl. BaHF platelets prepared by molten salt synthesis in varying flux compositions were mixed with the PS matrix, and composites were obtained by tape casting. In the composites containing BaHF powders synthesized by mixed oxide method, the highest EM wave absorption was achieved by the addition of 30 wt% BaHF. Because of this reason, 30 wt% BaHF was chosen as the BaHF platelet content to be added in the PS matrix. Reflection and transmission loss of the composites containing BaHF platelets synthesized in 5 different flux compositions are given in Figure 4.25. Reflection loss of the composites changes between -20 and -10 dB for all flux compositions.

Specifically, composite containing platelets synthesized in 100 wt% NaCl reveals a reflection loss around -15 dB throughout the whole frequency range. Transmission loss of all composites changes between about -3 and -1 dB independent of the flux composition.

EM wave absorption of the composites containing BaHF platelets synthesized in 5 different flux compositions is given in Figure 4.26. As discussed in the earlier sections, BaHF platelets synthesized in varying fluxes reveal different morphologies, phase contents and hence magnetic properties. The effect of these differences reveals itself in the EM wave absorption properties of the composites. BaHF platelets synthesized in 100 wt% NaCl flux has the highest magnetic coercivity and magnetic remanence, which results in the highest EM wave absorption reaching to about 25% based on the highest magnetic loss achieved in the BaHF platelets synthesized in 100 wt% NaCl composition.

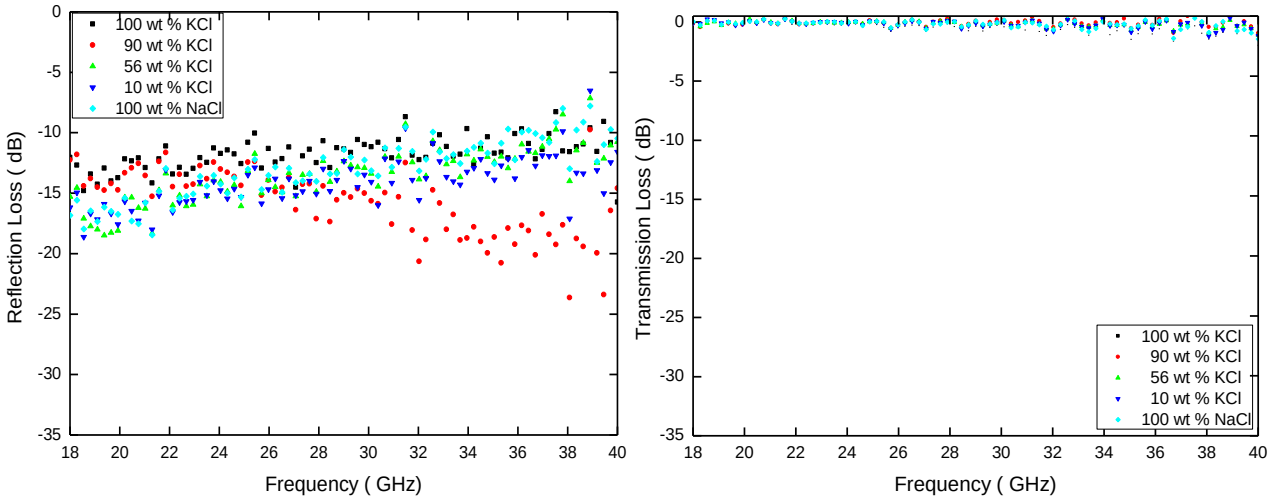

Figure 4.25 EM wave reflection and transmission losses of composites containing BaHF platelets synthesized in 5 different flux compositions.

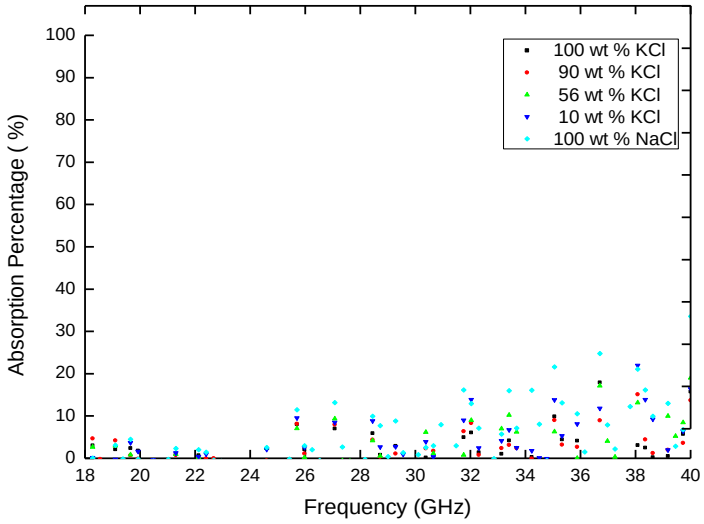

Figure 4.26 EM wave absorption of composites containing BaHF platelets synthesized in 5 different flux compositions.

To reveal the effect of tape casting on the EM wave properties of BaHF platelet containing composites, composite samples were prepared in tape-cast and as-cast form each containing 30 wt% BaHF platelets synthesized in 100 wt% NaCl. This specific flux composition was chosen based on the highest EM wave absorption achieved in composites containing platelets synthesized in it. Reflection and transmission losses of these tape-cast and as-cast composites are given in Figure 4.27. As it is clear from this figure, as-cast composite reveals lower reflection loss compared to tape-cast composite, which is opposite in the case of their transmission loss that is nearly at the same magnitude. This shows that tape casting promotes lower reflection by the alignment of the platelets it provides, while its transmission loss is comparable to that of the as-cast composite. Consequently, tape-cast composite reveals higher EM wave absorption as shown in Figure 4.28.

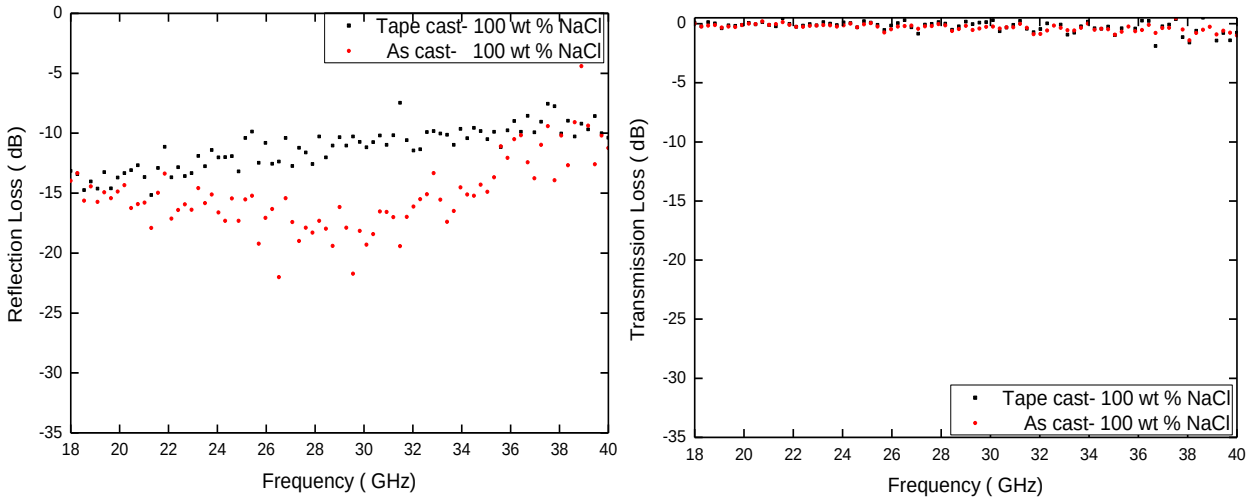

Figure 4.27 EM wave reflection and transmission losses of tape-cast and as-cast composites containing BaHF platelets.

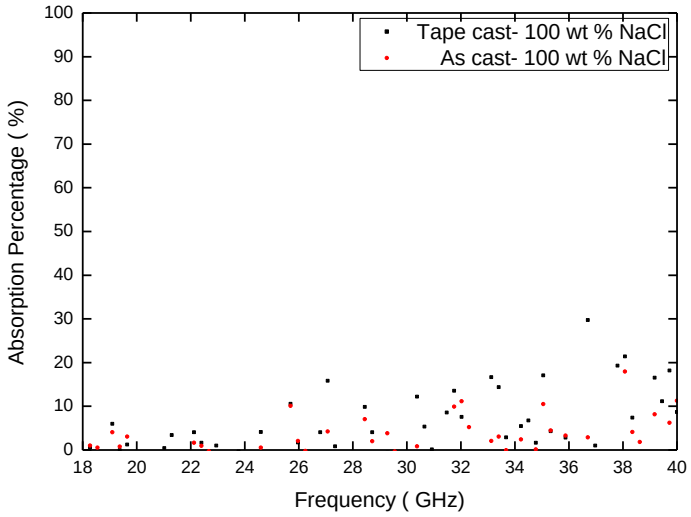

Figure 4.28 EM wave absorption of tape-cast and as-cast composites containing BaHF platelets.

4.7.3 BaHF Powder - Graphite or Ni Flake/ PC Matrix Composites

Based on the magnetic losses they provide BaHF powders are more effective fillers for EM wave absorbing composites active at the end of MHz and at the beginning of GHz frequency regions. However, the free-space measurement setup used in this study works at higher frequencies, as a result the EM wave absorption properties of BaHF powder and BaHF platelet containing PS composites were not at desired level both in their tape-cast and as-cast forms. In order to modify and improve the EM absorption potential of BaHF based composites, graphite or nickel flakes were added to a polymer matrix, PC, along with BaHF powders synthesized by mixed oxide method. With the addition of these flake shaped electrically conducting fillers, ohmic loss was intended to be incorporated into the composite beside the magnetic loss provided by the BaHF powders.

Furthermore, alignment of the flake shaped fillers was aimed to be achieved by tape casting to improve the EM wave absorption potential of the resulting composites. BaHF powder-Graphite Flake/PC matrix and BaHF powder-Ni Flake/PC matrix composites were obtained separately by tape casting. Following this 6.5 x 6.5 cm big, square shaped 8 specimens were cut out of these tapes.

The specimens of each composite tape type were cascaded after each other, and EM wave reflection loss, transmission loss and absorption of 1 to 8 layered composites were measured using the formerly mentioned free-space setup in 18-40 GHz frequency range.

4.7.3.1 BaHF Powder – Graphite Flake/PC Composites

Reflection and transmission loss of the BaHF powder and graphite flake containing PC matrix composites are given in Figure 4.29 for 1 up to 8 layer tapes cascaded after each other. As it is clear from this figure, transmission loss decreases with increasing number of tapes pointing out to the lower amount of transmission through the multilayered composite material. This is expected, since with the increasing number of tapes the medium is getting richer in terms of the lossy filler content suppressing the transmission of the EM waves.

However, unexpectedly this is just the opposite in the case of the reflection loss. Reflection loss of the composite decreases with the increasing number of tapes in the multilayered structure. This unexpected tendency appears even though the conducting filler content in the composite medium increases with increasing number of layers. The decrease in the reflection despite the increase in the conducting filler content in the medium can be attributed to the multiple scattering of the EM waves within the multilayered composite structure formed by individual tapes.

The reflection loss of 8 layered composite changes between about -25 and -17 dB in the frequency range under interest, where its transmission loss changes between -3 and -5 dB in the same frequency range.

As the main target is to minimize both EM wave reflection and transmission simultaneously in order to achieve maximum EM wave absorption, the 8 layered composite seems to have an optimum combination in terms of this target.

Consequently, as it is seen in Figure 4.30, the 8 layered composite reveals the maximum EM wave absorption changing between ~30-70% in the frequency range under interest..

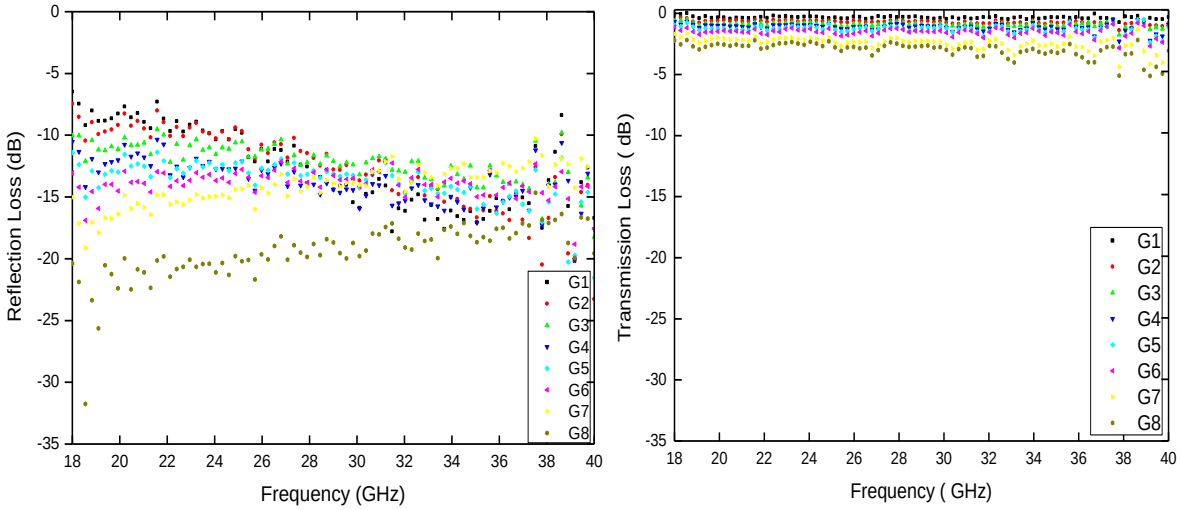

Figure 4.29 EM wave reflection and transmission losses of BaHF powder and graphite flake containing PC matrix composites for varying number of tapes cascaded to form the multilayered structure.

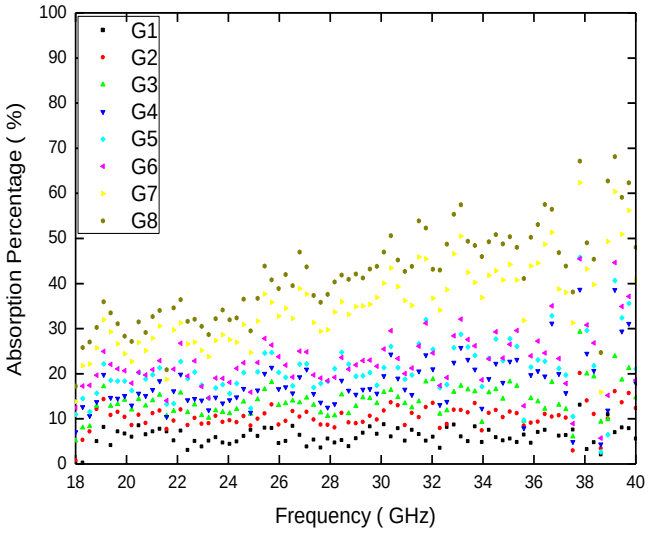

Figure 4.30 EM wave absorption of BaHF powder and graphite flake containing PC matrix composites for varying number of tapes cascaded to form the multilayered structure.

4.7.3.2. BaHF Powder - Ni Flake/PC Composites

Reflection and transmission loss of the BaHF powder and Ni flake containing PC matrix composites are given in Figure 4.31 for 1 up to 8 layer tapes cascaded after each other. Unlike the case with the graphite flake containing composites (Figure 4.29), reflection loss of Ni flake containing composites increases with increasing number of tapes cascaded in multilayer form. This is somehow expected as the amount of the conducting filler increases the composite medium becomes more reflective against the EM waves.

Here it should be noted that as demonstrated earlier unlike the graphite flake containing ones Ni flake containing tapes do not reveal a measurable conductivity. This seems to be contradicting with the increasing reflection loss with increasing number of Ni flake containing tapes. Absence of electrical conduction in Ni flake containing tapes points out to the lack of network formation and hence percolation of Ni flakes.

However, despite their lack of electrical conductivity increasing reflection loss of Ni flake containing tapes with their increasing number shows that rather than a conducting network, presence of locally conducting domains in the tape structure can also provide lossy character. Ferromagnetic nature of the Ni has to be also considered at this point which might be contributing this lossy character. The reason behind this unexpected relation and occurrence can be explained within the scope of a further study involving the modeling of the EM wave interaction characteristics and electrical properties of such discontinuous media.

Transmission loss of Ni flake containing composites decreases with increasing number tapes in the cascaded structure. This tendency is in good correlation with the increasing reflection loss, since the reflective media are normally expected to be less transmitting against the EM waves. Consequently, both the reflection and transmission loss of the 8 layered cascaded structure changes between -5 and -10 dB for the frequency range investigated.

This balanced reflection and transmission behavior of this 8 layered structure results in the maximum absorption changing between 50 and 75% in 18-40 GHz frequency range (Figure 4.32).

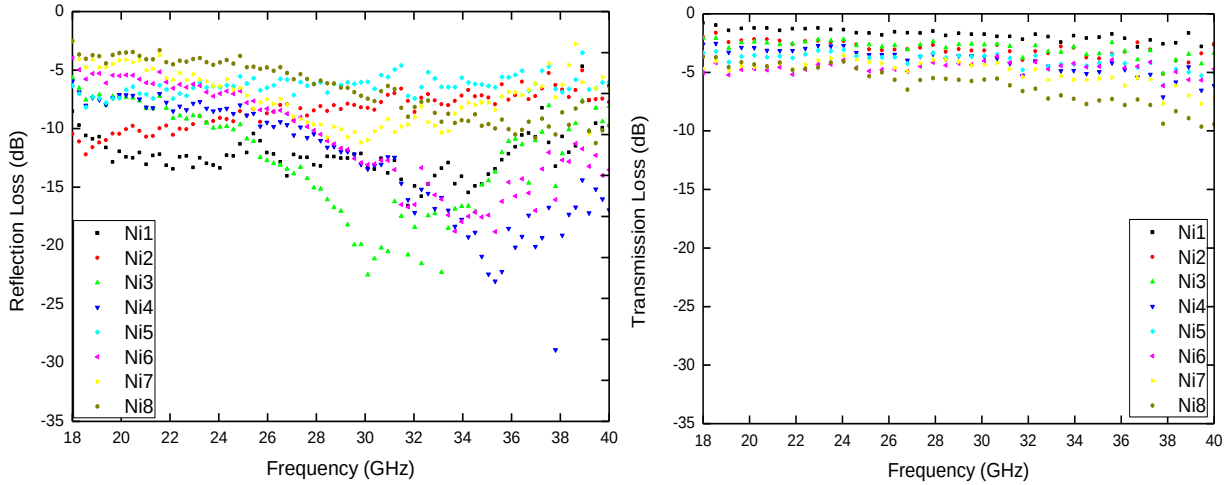

Figure 4.31 EM wave reflection and transmission losses of BaHF powder and Ni flake containing PC matrix composites for varying number of tapes cascaded to form the multilayered structure.

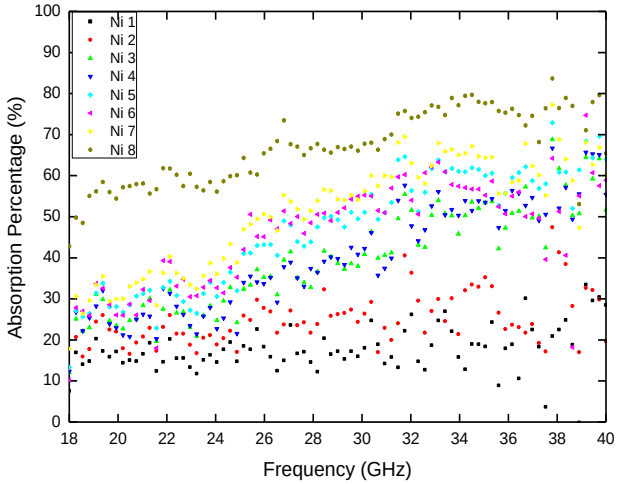

Figure 4.32 EM wave absorption of BaHF powder and Ni flake containing PC matrix composites for varying number of tapes cascaded to form the multilayered structure.

CHAPTER 5

5. CONCLUSIONS

In BaHF-based electromagnetic (EM) wave absorbing polymer matrix composites, BaHF powders and platelets were used. Mixed oxide method was applied to synthesize nano meter size BaHF powders, while micron size BaHF platelets were prepared by molten-salt synthesis method in various weight proportions of NaCl–KCl salt mixtures.

X-Ray diffraction analysis (XRD), scanning electron microscopy (SEM) and vibrating sample magnetometer (VSM) were used to identify the characteristics of the synthesized BaHF platelets. The effect of molten salt composition on the amount of BaHF phase formation, as well as, on the morphology and magnetic properties of the final products were discussed according to the results obtained from the characterization tools.

BaHF-based polymer matrix composites were prepared by tape casting method, and their EM wave absorption potentials were investigated within 18-40 GHz frequency range by free-space measurement method. In order to enhance the EM wave absorption potential of BaHF-based polymer matrix composites, graphite or Ni flakes were incorporated in the composites together with BaHF powders. Composites were fabricated by tape casting and cascading the obtained tapes after each other forming a multilayered composite structure. EM wave absorbing multilayered composites were characterized in terms of their EM wave reflection and transmission losses along with their EM wave absorption.

Following points demonstrate the major conclusions drawn at the end of this study:

- In molten salt synthesis method, BaHF platelet size in NaCl flux was larger than that in KCl for all the calcination temperatures and durations applied. This demonstrates the lower apparent activation energy for platelet growth in NaCl rich fluxes.

- Compared to other temperatures, platelets synthesized in 90 wt% NaCl containing flux had the largest platelet size of ~2 μm at 900 °C for 2 h calcination duration.

- For the morphology of the BaHF platelets, in the case of the synthesis at 900 °C in NaCl flux, corners of the platelets became rounded. This is speculated to be caused by the selective desorption from the corners of the platelets as a result of chemical potential change around the sharp corners of the platelets in the molten NaCl flux. In the case of platelet synthesis in KCl flux, either no desorption occurred or desorption occurred homogenously on all the surfaces and corners of the platelets so that platelet shape with sharp corners was preserved.

- Quantitative XRD results showed that NaCl plays a prominent role on the formation of BaHF phase. As the content of NaCl in the flux increases, BaHF formation is enhanced. The highest conversion which is 97.8% is obtained in the case of synthesis in 100 wt% NaCl flux.

- Flux composition has clear impact on the magnetic properties of BaHF platelets mainly based on the efficiency of transformation. Increasing NaCl content in the flux improves the coercivity and remnant magnetization of BaHF along with the area under the hysteresis curve leading to a more pronounced hard magnetic behavior in the synthesized ceramics.

- In the case of the BaHF-based polymer matrix composites, as the content of BaHF in the structure increases, the electromagnetic absorption properties are enhanced. The highest EM wave absorption reaching to ~25% was obtained in 30 wt% BaHF containing composites.

- EM wave absorption of tape-cast composites are slightly higher than that of the as-cast ones caused by the texture or inorganic phase alignment formed during tape casting.

- Composites containing BaHF platelets synthesized in 100 wt% NaCl flux revealed the highest EM wave absorption values resulted from the magnetic loss provided by this platelets due to the highest magnetic coercivity and magnetic remanance they reach.

- In order to modify and improve the EM wave absorption properties of BaHF-based polymer matrix composites, graphite or Ni flakes were added to the composite together with the BaHF powders.

- Multilayered composites were prepared by cascading the composite tapes containing these inorganic mixtures, as a result enhanced EM wave absorption was obtained by the multiple interaction of EM waves reflected from and transmitted through successive layers.

- Because of the synergistic effect of the magnetic and ohmic loss provided by the nickel, BaHF-Ni flake composites revealed a balanced reflection and transmission behavior resulting in the maximum EM wave absorption achieved between 50 and 75% in 18-40 GHz frequency range.

REFERENCES

[1] Chin W. S and Lee D. G., "Development of the Composite RAS (radar absorbing structure) for the X-band frequency range," Compos. Struct. , vol. 77, pp. 457-465, (2007).

[2] Pinho M.S., Gregori M. L., Nunes R. C. R., and Soares B. G., "Performance of radar absorbing materials by waveguide measurements for X-and Ku- band frequencies.", Eur. Polym. J., vol. 38, pp. 2321-2327, (2002).

[3] Huang C. Y., Mo W. W., and Roan M. L., "Studies on the influence of double-layer electroless metal deposition on the electromagnetic interference shielding effectiveness of carbon fiber/ABS composites." Surf. Coat. technol., vol. 184, pp. 163-169, (2004).

[4] Shui X.P. and Chung D. D.L., " Submicron diameter nickel filaments and their polymer-matrix composites," J. Mater. Sci., vol. 35, pp. 1773-1785, (2000).

[5] Tzeng S. S. and Chang F. Y, " EMI shielding effectiveness of metal-coated carbon fiber-reinforced ABS composites.", Mater. Sci. Eng., A, vol. 302. pp. 258-267, (2001).

[6] Wu. J. and Chung D.D. L., "Increasing the electromagnetic interference shielding effectiveness of carbon fiber polymer-matrix composite by using activated carbon fibers." Carbon, vol. 40. pp. 445-447, (2002).

[7] Zhano N., Zou T., Shi C. Li J. and Guo W., "Microwave absorbing properties of activated carbon-fiber felt screens (vertical-arranged carbon fibers/epoxy resin composites." Mater. sc. Eng., B, vol. 127, pp. 207-211, (2006).

[8] Park K. Y., Lee S. E., Kim C. G., and Han J. H., "Fabrication of electromagnetic characteristics of electromagnetic wave absorbing sandwich structures," Comp. Sci. Technol., vol. 66. pp. 576-584, (2006).

[9] Oh J. H., Oh K. S., Kim C. G., and Hong C. S., “Design of radar absorbing structures using glass/epoxy composite containing carbon black in X-band frequency ranges.” Composites Part B, vol. 35. pp. 49-56, (2004).

[10] Y. Liu, M.G.B. Drew, J. Wang, M. Zhang “Preparation, characterization and magnetic properties of the doped barium hexaferrites BaFe12−2xCox/2Znx/2SnxO19, x=0.0−2.0”, Journal of Magnetism and Magnetic Materials, pp. 814–818, 322 (7) (2010).

[11] M.C. Dimri, S.C. Kashyap, D.C. Dube, “ Electrical and magnetic properties of barium hexaferrite nanoparticles prepared by citrate precursor method”, Ceramics International, 30 (7) pp. 1623–1626, (2004).

[12] W. Roos, “ Formation of chemically coprecipitated barium ferrite”, Journal of the American Ceramic Society, 63 (11–12) pp. 601–603, (1980).

[13] D. Barb, L. Diamandescu, A. Rusi, D. TA˘rA˘bA˘sanu-MihA˘ilA˘, M. Morariu, V. Teodorescu, “ Preparation of barium hexaferrite by a hydrothermal method: structure and magnetic properties”, Journal of Materials Science, 21 (4) pp. 1118–1122, (1986).

[14] S. Singhal, T. Namgyal, J. Singh, K. Chandra, S. Bansal, “ A comparative study on the magnetic properties of $MFe_{12}O_{19}$ and $MAlFe_{11}O_{19}$ (M=Sr, Ba and Pb) hexaferrites with different morphologies”, Ceramics International, 37 (6) pp. 1833–1837, (2011).

[15] E.K. Akdogan, R.E. Brennan, M. Allahverdi, A. Safari, “ Effects of molten salt synthesis (MSS) parameters on the morphology of Sr3Ti2O7 and SrTiO3 seed crystals”, Journal of Electroceramics, 16 (2) pp. 159–165, (2006).

[16] R.H. Arendt, J.H. Rosolowski, J.W. Szymaszek, “Lead zirconate titanate ceramics from molten salt solvent synthesized powders”, Materials Research Bulletin, 14 (5) pp. 703–709, (1979).

[17] J.P. Wang, Y. Liu, M. Hu, M.L. Zhang, “ Effects of different molten-salt on the synthesis of hexagonal barium ferrite”, Chinese Journal of Aeronautics, 19 pp. S206–S209, (2006).

[18] S. Dursun, R. Topkaya, N. Akdoan, S. Alkoy, " Comparison of the structural and magnetic properties of submicron barium hexaferrite powders prepared by molten salt and solid state calcination routes", Ceramics International, 38 (5) pp. 3801–3806, (2012).

[19] Neelkanta P.S., "Handbook of Electromagnetic Materials: Monolithic and Composite Versions and Their Applications", CRC-Press, (1995). Pp:491, Chapter 22.

[20] Retrieved on 1 st of January, 2014 from,
http://www.emiguru.com/blogpix/shieldpix_150x150_p1.jpg

[21] Knott E.F., Shaeffer J. F and Tuley M. T., "Radar Cross Section", Aztech House Inc., 2 nd Edition (1993). Pp:9,10

[22] Chin W. S. and Lee D. G., Composite Structures, Article in Press (2005).

[23] Chin W. S and Lee D. G., " Development of the Composite RAS (radar absorbing structure) for the X-band frequency range," Compos. Struct. , vol. 77, pp. 457-465, (2007).

[24] Seo I. S., Chin W. S. and Lee D. G., Composite Structures 665, 33-542 (2004).

[25] Wang C. M. B. and Li Q., Materials and Design, 19 113-120 (1998).

[26] Ghasemi A., Hossienpour A., Morisako A., Saatchi A. and Salehi M., Journal of Magnetism and Magnetic Materials, Article in Press (2005).

[27] Wang C., Li L., Zhou J., Qi X., Yue Z. and Wang X., Journal of Magnetism and Magnetic Materials, pp. 100-106 (2002).

[28] Rezende M. C., Martin I. M., Milacci M. A. S., and Nohara E.L., " Radar cross section measurements (8-12 GHz) of flat plates painted with microwave absorbing materials," IEEE, vol. 1, pp. 263-267, (2001).

[29] Amin M. B. and James J. R., The radio and Electronic Engineer, Part 1 pp. 209-218, (1981).

[30] Weir W. B. ," Automatic measurement of complex dielectric constant and permeability at microwave frequencies," IEEE, pp. 33-36, (1974).

[31] Biscaro R. S., Nohara E. L., Peixoto G. G., Faez R., and Rezende M. C., " Performance evaluation of conducting polymer paints as radar absorbing materials," IEEE, pp. 355-358, (2003).

[32] Pinho M.S., Gregori M. L., Nunes R. C. R., and Soares B. G., " Performance of radar absorbing materials by waveguide measurements for X-and Ku- band frequencies.", Eur. Polym. J., vol. 38, pp. 2321-2327, (2002).

[33] Huang C. Y., Mo W. W., and Roan M. L., "Studies on the influence of double-layer electroless metal deposition on the electromagnetic interference shielding effectiveness of carbon fiber/ABS composites." Surf. Coat. technol., vol. 184, pp. 163-169, (2004).

[34] Shui X.P. and Chung D. D.L., " Submicron diameter nickel filaments and their polymer-matrix composites," J. Mater. Sci., vol. 35, pp. 1773-1785, (2000).

[35] Tzeng S. S. and Chang F. Y, " EMI shielding effectiveness of metal-coated carbon fiber-reinforced ABS composites.", Mater. Sci. Eng., A, vol. 302. pp. 258-267, (2001).

[36] Wu. J. and Chung D.D. L., " Increasing the electromagnetic interference shielding effectiveness of carbon fiber polymer-matrix composite by using activated carbon fibers." Carbon, vol. 40. pp. 445-447, (2002).

[37] Zhano N., Zou T., Shi C. Li J. and Guo W., "Microwave absorbing properties of activated carbon-fiber felt screens (vertical-arranged carbon fibers/epoxy resin composites." Mater. sc. Eng., B, vol. 127, pp. 207-211, (2006).

[38] Park K. Y., Lee S. E., Kim C. G., and Han J. H., "Fabrication of electromagnetic characteristics of electromagnetic wave absorbing sandwich structures," Compos. Sci. Technol. , vol. 66. pp. 576-584, (2006).

[39] Oh J. H., Oh K. S., Kim C. G., and Hong C. S., " Design of radar absorbing structures using glass/epoxy composite containing carbon black in X-band frequency ranges." Composites Part B vol. 35. pp. 49-56, (2004).

[40] Saville P., " A review of optimisation techniques for layered radar absorbing materials," Technical Memorandum, Atlantic, 2004.

[41] Bhattacharyya A., Sengupta D. L., " Radar cross section analysis and control," Artech House, 1991.

[42] Marshall S. V. and Skitek G. G., " Electromagnetic concepts and applications," Prentice hall, New Jersey, 3 rd Edition, (1990).

[43] Valenzuela R., " Magnetic ceramics," Cambridge University Press, (1994).

[44] McCurrie R. A., " Ferromagnetic materials: structure and properties," Academic Press, London. (1994).

[45] Smith J., Wijn H. P. J., "Ferrites", New York, Wiley, (1959).

[46] Kaiser M., "Influence of V2O5 ion addition on the conductivity and grain growth of Ni–Zn–Cu ferrites," Current Applied Physics 10 (4) 975-984. (2010).

[47] Özgür Ü., Alivov Y., Morkoç H., "Microwave ferrites, " Part 1: Fundamental properties, J Mater Sci: Mater Electron 20 (9) 789-834, (2009).

[48] E.Aydogan, S.Kaya, A. F. Dericioglu, "Morphology and Magnetic Properties of Barium Hexaferrite Ceramics Synthesized in x wt% NaCl-(100-x) wt% KCl Molten Salts", Ceramics International, 40, 2331-2336, (2014).

[49] B.T. Shirk, W.R.Buessem, "Temperature Dependence of M_s and K_1 of $BaFe_{12}O_{19}$ and $SrFe_{12}O_{19}$ Single Crystals, *J.Appl.Phys.***40**, 1294(1969).

[50] K.Haneda, H.Kojima, "Magnetization reversal process in chemically precipitated and ordinary prepared $BaFe_{12}O_{19}$", *J.Appl.Phys*. **44**,3760(1973).

[51] Winkler G., " Crystallography, chemistry and technology of ferrites. In magnetic properties of materials," McGraw-Hill, London, (1971).

[52] Retrieved on 1 st of January, 2014 from,
http://origin-ars.els-cdn.com/content/image/1-s2.0-S0304885304002793-gr1.jpg

[53] Louh R., Reynolds III T. G., Buchanan R. C., " Ferrite ceramics in ceramic materials for electronics," Marcel Dekker Inc., Newyork, (2004).

[54] Retrieved on 1 st of January, 2014 from
http://www.doitpoms.ac.uk/tlplib/ferromagnetic/types.php

[55] Moulson A. J., Herbert J. M., " Electroceramics: Materials, properties, applications," John Wiley & Sons Ltd., (2003).

[56] RF Absorbers Catalog, Advanced ElectroMagnetics, Inc., Santee, CA, (2011).

[57] Sugimoto M, "The Past, Present, and Future of Ferrites", Journal of the American Ceramic Society, Volume 82, Issue 2, Article first published online: 22 DEC 2004

[58] Hsiang H-I, Chang C-H, "Molten salt synthesis and magnetic properties of $3BaO{\cdot}2CoO{\cdot}12Fe_2O_3$ powder", Journal of Magnetism and Magnetic Materials, 278 218-222, (2004).

[59] He1 X, Zhong1 W, Yan1 S, Au2 C-T, L ¨u1 L and Du1 Y, "The structure, morphology and magnetic properties of Sr-ferrite powder prepared by the molten-salt method", J. Phys. D: Appl. Phys. 47 235002 (10pp), (2014).

[60] Abbas S. M., Chatterjee R., "Electromagnetic and microwave absorption properties of (Co2+-Si4+) substituted barium hexaferrites and its polymer composite," Journal of Applied Physics 101(7), (2007).

[61] Wu Y. P., Ong C. K.,"Improved microwave magnetic and attenuation properties due to the dopant V2O5 in W-type barium ferrites.", Journal of Physics D-Applied Physics 39(14), 2915-2919, (2006).

[62] Wu Y., Huang Y., "Several W-type barium ferrites with different Me2: Preparation and the electromagnetic properties.", Cailiao Yanjiu Xuebao/Chinese Journal of Materials Research 25(6), 607-612, (2011).

[63] Tehrani M. K., Ghasemi A., "Wideband electromagnetic wave absorber using doped barium hexaferrite in Ku-band.", Journal of Alloys and Compounds, 509(33), 8398-8400, (2011).

[64] Liangchao L, Chen K., "Attractive microwave-absorbing properties of M-BaFe12O19 ferrite.", Journal of Alloys and Compounds, 557(0), 11-17, (2013).

[65] Retrieved on 2 nd of January, 2014 from http://weblog.sirajs.com/article/magnetic-properties-materials

[66] Smith W. F., " Principles of materials science and engineering," McGraw-Hill, 3 rd Edition, Chapter 11 Magnetic Materials, (1996).

[67] Retrieved on 11 th of November, 2013 from http://commons.wikimedia.org/wiki/File:BH_Curve_and_Loop.jpg

[68] R.H.Arendt," Liquid-phase sintering of magnetically isotropic and anisotropic compacts of $BaFe_{12}O_{19}$ and $SrFe_{12}O_{19}$", Journal of Applied Physics, 44(7), 3300, (1973).

[69] Y.T.Chien, H.C.Pan,"Preparation and Properties of Barium Ferrite Using Hot-Rolled Mill Scale ", Journal of American Ceramic Society 72(8) (1989) 1328-1332.

[70] Retrieved on 1 st of January, 2014 from http://www.crct.polymtl.ca/fact/phase_diagram.php?file=KCl-NaCl.jpg&dir=FTsalt

[71] Steve J. Chipera, David L. Bish, "Fitting Full X-Ray Diffraction Patterns for Quantitative Analysis: A Method for Readily Quantifying Crystalline and Disordered Phases", Advances in Materials Physics and Chemistry, 3, 47-53, (2013).

[72]Retrieved on 10 th of June, 2014 from http://nanolab.berkeley.edu/labmanual/chap8/8.024ptprb2.pdf

[73]Retrieved on 10 th of June, 2014 from http://www.imagesco.com/articles/superconductors/four-pt-schematic.gif

[74] N. Gagnon, “Design and Study of a Free - Space Quasi Optical Measurement System, in "Institute for Electrical and Computer Engineering" (University of Ottawa, Ottawa, 2002).

[75]Retrieved on 10 th of June, 2014 from http://www.tibtech.com/conductivity.php

[76]Retrieved on 8 th of June, 2014 from http://chemistry.stackexchange.com/questions/820/electrical-conductivity-of graphite.